

1 **ShellChron 0.2.84.0: A new tool for constructing chronologies in accretionary carbonate**
2 **archives from stable oxygen isotope profiles**

3 Niels J. de Winter^{1,2}

4 ¹Department of Earth Sciences, Utrecht University, Utrecht, the Netherlands

5 ²AMGC research group, Vrije Universiteit Brussel, Brussels, Belgium

6

7 Corresponding author: Niels J de Winter (n.j.dewinter@uu.nl)

8

9

10

11 **Abstract**

12 This work presents ShellChron, a new model for generating accurate internal age-~~depth~~-models for high-
13 resolution paleoclimate archives, such as corals, mollusk shells and speleothems. Reliable sub-annual
14 age models form the backbone of high-resolution paleoclimate studies. In absence of independent sub-
15 annual growth markers in many of these archives, the most reliable method for determining the age of
16 samples is through age modelling based on stable oxygen isotope or other seasonally controlled proxy
17 records. ShellChron expands on previous solutions to the age model problem by ~~modelling-fitting a~~
18 combination of a growth rate and temperature sinusoid to model seasonal variability in the proxy record
19 ~~using a combination of growth rate and temperature sinusoids~~ in sliding window approach. This new
20 approach creates smoother, more precise age-~~depth-distance~~ relationships for multi-annual proxy
21 records with the added benefit of allowing assessment of the uncertainty on the modelled age. The
22 modular script of ShellChron allows the model to be tailored to specific archives, without being limited
23 to oxygen isotope $\delta^{18}\text{O}_\text{c}$ -proxy records or carbonate archives, with high flexibility in assigning the
24 relationship between the input proxy and the seasonal cycle. The performance of ShellChron in terms
25 of accuracy and computation time is tested on a set of virtual seasonality records and real coral, bivalve
26 and speleothem archives. The result shows that several key improvements in comparison to previous
27 age model routines enhance the accuracy of ShellChron on multi-annual records while limiting its

28 processing time. The current full working version of ShellChron enables the user to model the age of a
29 10-year long high-resolution (16 samples/yr) carbonate records with monthly accuracy within one hour
30 of computation time on a ~~modern~~ personal computer. The model is freely accessible on the CRAN
31 database and GitHub. Members of the community are invited to contribute by adapting the model code
32 to suit their research topics.

33

34

35 1. Introduction

36 Fast growing carbonate archives, such as coral skeletons, mollusk shells and speleothems, contain a
37 wealth of information about past and present climate and environment (e.g. Urban et al., 2000; Wang et
38 al., 2001; Steuber et al., 2005; Butler et al., 2013). Recent advances in analytical techniques have
39 improved our ~~cap~~ability to extract this information and obtain records of the conditions under which these
40 carbonates precipitated at high ~~time-temporal~~ resolutions, often beyond the annual scale (Treble et al.,
41 2007; Saenger et al., 2017; Vansteenberghe et al., 2019; de Winter et al., 2020a). Key to the interpretation
42 of such records is the development of reliable chemical or physical proxies for climate and environmental
43 conditions which can be measured on a sufficiently fine scale to allow variability to be reconstructed at
44 the desired time resolution. Examples of suitable proxies include observations of variability in carbonate
45 fabric and microstructure and in (trace) elemental and isotopic composition (Frisia et al., 2000; Lough,
46 2010; Ullmann et al., 2010; Schöne et al., 2011; Ullmann et al., 2013; Van Rempelbergh et al., 2014; de
47 Winter et al., 2017). The unique preservation potential of carbonates in comparison with archives of
48 climate variability at similar time resolutions, such as tree ring records and ice cores, now allows us to
49 recover information about climate and environment of the geological past from these proxies on the
50 (sub-)seasonal scale (Ivany and Runnegar, 2010; Ullmann and Korte, 2015; Vansteenberghe et al., 2016;
51 de Winter et al., 2018; 2020b; c; Mohr et al., 2020). The importance of this development cannot be
52 overstated because variability at high (daily and seasonal) resolution constitutes the most significant
53 component of climate variability (Mitchell, 1976; Huybers and Curry, 2006; Zhu et al., 2019). Accurate
54 reconstructions of this type of variability are therefore fundamental to our understanding of Earth's
55 climate system and critical for projecting ~~of~~-its behavior in the future under ~~greenhouse-anthropogenic~~
56 ~~global~~ warming conditions (IPCC, 2018).

57 A reliable age model is crucial to the interpretation of high-resolution carbonate records. An age model
58 is defined as a set of rules or markers that allows the translation of the location of a measurement or
59 observation on the archive to the time by-at which the carbonate was precipitated. This translation is
60 required for aligning records from multiple proxies or archives to a common time axis. Age alignment
61 enables data to be intercomparable and to be interpreted in the context of processes playing a role at
62 similar timescales. Age models are based on knowledge about the growth or accretion rate of the archive
63 through time. Many high-resolution carbonate archives contain growth markers on which age models
64 can be based (e.g. Jones, 1983; Le Tissier et al., 1994; Verheyden et al., 2006). These are especially
65 valuable in some mollusk species, in which growth lines demarcate annual, daily, or even tidal cycles
66 (e.g. *Arctica islandica*, Schöne et al., 2005; *Pecten maximus*, Chavaud et al., 2005 and *Cerastoderma*
67 *edule*, Mahé et al., 2010). However, in many mollusk species and most carbonate archives, such
68 independent growth indicators are absent or too infrequent to (relatively) date high-resolution
69 measurements (Judd et al., 2018; Huyghe et al., 2019). In such cases, age models need to be based
70 on alternative indicators.

71 The oxygen isotope composition of carbonates ($\delta^{18}\text{O}_c$) is closely dependent on the isotopic composition
72 of the fluid ($\delta^{18}\text{O}_w$) and the temperature by-at which the carbonate is precipitated (Urey, 1948; McCrea,
73 1950; Epstein et al., 1953). In most natural surface environments, either one or both factors is strongly
74 dependent on the seasonal cycle, one generally being dominant over the other. This causes carbonates
75 precipitated in these environments to display strong quasi-sinusoidal variations in $\delta^{18}\text{O}_c$ that follow the
76 seasonal cycle (e.g. Dunbar and Wellington, 1981; Jones and Quitmyer, 1996; Baldini et al., 2008).
77 Examples of this behavior include seasonal cyclicity in sea surface temperatures recorded in the $\delta^{18}\text{O}_c$
78 of corals and mollusks and seasonal cyclicity in the $\delta^{18}\text{O}_w$ of precipitation recorded in speleothems
79 (Dunbar and Wellington, 1981; Schöne et al., 2005; Van Rampelbergh et al., 2014). This relationship is
80 challenged in tropical latitudes, where temperature seasonality is restricted. However, in some tropical
81 archives, the annual cycle of $\delta^{18}\text{O}_w$ in precipitation still allows the annual cycle to be resolved from $\delta^{18}\text{O}$
82 records (e.g. Evans and Schrag, 2004). These properties make $\delta^{18}\text{O}_c$ one of the most highly sought-
83 after proxies for climate variability, and high-resolution $\delta^{18}\text{O}_c$ records are abundant in the paleoclimate
84 literature (e.g. Lachniet, 2009; Lough, 2010; Schöne and Gillikin, 2013 and references therein).

85 The close relationship between $\delta^{18}\text{O}_c$ records and the seasonal cycle can also be exploited to estimate
86 variability in growth rate of the archive. This property of $\delta^{18}\text{O}_c$ curves has been recognized by previous

87 authors, and attempts have been made to quantify intra-annual growth rates from the shape of $\delta^{18}\text{O}_c$
88 profiles (Wilkinson and Ivany, 2002; Goodwin et al., 2003; De Ridder et al., 2006; Goodwin et al., 2009;
89 De Brauwere et al., 2009; Müller et al., 2015; Judd et al., 2018). Over time, these so called "growth
90 models" have improved from fitting of sinusoids to $\delta^{18}\text{O}_c$ data (Wilkinson and Ivany, 2002; De Ridder et
91 al., 2006) to including increasingly complicated (inter)annual growth rate curves to the model to fit the
92 shape of the $\delta^{18}\text{O}_c$ data (Goodwin et al., 2003; 2009; Müller et al., 2015; Judd et al., 2018). These later
93 models manage to fit the shape of $\delta^{18}\text{O}_c$ records well, but they often rely on detailed *a priori* knowledge
94 of growth rate or temperature patterns (e.g. Goodwin et al., 2003; 2009), which ~~causes them to rely~~
95 ~~on~~requires measurements of one or more parameters in the environment. These measurements are not
96 available in studies on carbonate archives from the archeological or geological past. In contrast, the
97 latest model by Judd et al. (2018) is based only on the assumption that growth and temperature follow
98 quasi-sinusoidal patterns and can therefore work with $\delta^{18}\text{O}_c$ data alone, making it more widely
99 applicable. The simplified parameterization of temperature and growth rate seasonality by Judd et al.
100 (2018) using two (skewed) sinusoids is demonstrated to approximate natural circumstances very well.

101 However, the approach by Judd et al. (2018) is still limited in its use, because it requires whole, individual
102 growth years to be analyzed separately, resulting in a discontinuous time series when applied on records
103 containing multiple years of $\delta^{18}\text{O}_c$ data and no solution for incomplete years. In addition, the model has
104 no option to supply information about the less dominant factor that drives $\delta^{18}\text{O}_c$ values ($\delta^{18}\text{O}_w$ of sea
105 water in the case of mollusks and corals). Furthermore, only estimates from aragonite records are
106 supported, while the other dominant carbonate mineral, calcite, has a different temperature relationship
107 (Kim and O'Neil, 1997). Finally, neither of the models highlighted above except for the MoGroFun model
108 by Goodwin et al. (2009) include any assessment of the uncertainty of the constructed age model.

109 Here, a new model for estimating ages of samples in seasonal $\delta^{18}\text{O}_c$ curves is presented which
110 combines the advantages of previous models while attempting to negate their disadvantages.
111 ShellChron combines a skewed growth rate sinusoid with a sinusoidal temperature curve to model $\delta^{18}\text{O}_c$
112 using the Shuffled Complex Evolution model developed at the University of Arizona (SCEUA;
113 ~~optimization algorithm~~ (Duan et al., 1992; following Judd et al., 2018). It applies this optimization using
114 a sliding window through the dataset (as in Wilkinson and Ivany, 2002) and includes the option to use a
115 Monte Carlo simulation approach to combine uncertainties on the input ($\delta^{18}\text{O}_c$ and ~~depth-sample~~
116 distance measurements) and the model routine (as in Goodwin et al., 2009). As a result, ShellChron

117 produces a continuous time series with a confidence envelope, supports records from multiple carbonate
 118 minerals and allows the user to provide information on the less dominant variable influencing $\delta^{18}\text{O}_c$ (e.g.
 119 $\delta^{18}\text{O}_w$) if available (see section 2). The modular design of ShellChron's functional script allows parts of
 120 the model to be adapted and interchanged, supporting a wide range of climate and environmental
 121 archives. As a result, the initial design of ShellChron for reconstructing age models in temperature-
 122 dominated $\delta^{18}\text{O}_c$ records from marine bio-archives (e.g. corals and mollusks) presented here can be
 123 easily modified for application on other types of records. The routine is worked out into a ready-to-use
 124 package for the open-source computational programming language R and is directly available without
 125 restrictions, allowing all interested parties to freely modify and build on the base structure to adapt it to
 126 their needs (R Core Team, 2020; full package code and documentation in **SI1**, see also **Code**
 127 **availability**).

128

129 2. Stable oxygen isotope profiles in carbonate archives: The scientific basis

130 The relationship between $\delta^{18}\text{O}_c$ and the temperature of carbonate precipitation was first established by
 131 Urey (1951) and later refined with additional measurements and theoretical models (Epstein et al., 1953;
 132 Tarutani et al., 1969; Grossman and Ku, 1986; Kim and O'Neil, 1997; Coplen, 2007; Watkins et al.,
 133 2014; Daëron et al., 2019). Empirical transfer functions for aragonite and calcite by Grossmann and Ku
 134 (1986; modified by Dettmann et al., 1999; **equation 1**) and Kim and O'Neil (1997; **equation 2**, with
 135 VSMOW to VPDB scale conversion following Brand et al., 2014; **equation 3**) have so far found most
 136 frequent use in modern paleoclimate ~~studies, and studies and~~ are therefore applied as default
 137 relationships in the ShellChron model (see *d18O_model* function).

$$138 \quad T[^\circ\text{C}] = 20.6 - 4.34 * (\delta^{18}\text{O}_c[\text{‰VPDB}] - \delta^{18}\text{O}_w[\text{‰VSMOW}] + 0.2) \quad (1)$$

$$139 \quad 1000 * \ln(\alpha) = 18.03 * \frac{10^3}{(T[^\circ\text{C}] + 273.15)} - 32.42$$

$$140 \quad \text{with } \alpha = \frac{\left(\frac{\delta^{18}\text{O}_c[\text{‰VPDB}]}{1000} + 1\right)}{\left(\frac{\delta^{18}\text{O}_w[\text{‰VPDB}]}{1000} + 1\right)} \quad (2)$$

$$141 \quad \delta^{18}\text{O}_w[\text{‰VPDB}] = 0.97002 * \delta^{18}\text{O}_w[\text{‰VSMOW}] - 29.98 \quad (3)$$

142 To apply these formulae, it is assumed that carbonate is precipitated in equilibrium with the precipitation
143 fluid. ~~The question w~~hich carbonates are precipitated in equilibrium has long been subject to debate,
144 and the development of new techniques for measuring the carbonate-water system (e.g. clumped and
145 dual-clumped isotope analyses; Daëron et al., 2019; Bajnai et al., 2020) has led recent authors to
146 challenge the assumption that equilibrium fractionation is the norm ([see Supplementary Discussion](#)).
147 ~~These recent findings suggest that kinetic effects in fast-growing carbonate archives or elevated pH in~~
148 ~~the calcification fluids of some calcifiers (e.g. foraminifera and corals; Rollion-Bard et al., 2003; Zeebe,~~
149 ~~2007) force precipitation out of equilibrium, and that true equilibrium is only reached in very slow-growing~~
150 ~~inorganic carbonates (e.g. Devils Hole vein calcite and subaqueous and cryogenic cave deposits;~~
151 ~~Coplen, 2007; Bajnai et al., 2020). On the other hand, disequilibrium fractionation likely affected the~~
152 ~~samples on which empirical transfer functions (equations 1 and 2) were based in a similar way as the~~
153 ~~samples on which they are applied, potentially eliminating the offset caused by disequilibrium~~
154 ~~fractionation (Daëron et al., 2019). In addition, the carbonic anhydrase enzyme present in many~~
155 ~~calcifiers accelerates CO₂ hydration at the calcification site, potentially eliminating kinetic effects in~~
156 ~~carbonate bio-archives whose growth rate would otherwise cause disequilibrium (Uchikawa and Zeebe,~~
157 ~~2012). These findings are corroborated by many studies of modern marine calcifiers such as mollusks~~
158 ~~and corals in which δ¹⁸O_c-based temperatures closely match *in situ* water temperatures (Dunbar and~~
159 ~~Wellington, 1981; Jones and Quitmyer, 1996; Ullmann et al., 2010; de Winter et al., 2020c). Therefore,~~
160 ~~it is widely assumed that many marine calcifiers precipitate their carbonates near isotopic equilibrium~~
161 ~~and that the empirical transfer functions yield accurate temperature reconstructions. Note that t~~The
162 modular character of ShellChron allows the empirical transfer function to be adapted to the δ¹⁸O_c record
163 or to the user's preference for alternative transfer functions by a small modification of the *d18O_model*
164 ~~function, and that f~~uture versions of the model will include more options for changing the transfer
165 ~~function by default~~ (see **Model description**).

166 As the name suggests, the ShellChron model was initially developed for application on δ¹⁸O_c records
167 from marine calcifiers (e.g. mollusk shells and corals). ShellChron approximates the **temperature**
168 **evolution of the calcification temperature** at which the carbonate is precipitated by a sinusoidal function
169 (see **equation 4, and Table 1, and SI4**; *temperature_curve* function; visualized in **Fig. 4A** and **Fig S1**),
170 a good approximation of seasonal temperature fluctuations in most marine and terrestrial environments
171 (Wilkinson and Ivany, 2002). Variability in δ¹⁸O_w is also comparatively limited in most marine

Formatted: Font: Not Bold

Formatted: Font: Not Bold

172 environments (except for regions with sea ice formation), making the model easy to use in these settings
173 (LeGrande and Schmidt, 2006; Rohling, 2013). Nevertheless, ShellChron includes the option to provide
174 a ~~priority-priori~~ knowledge about $\delta^{18}\text{O}_w$, ranging from annual average values to detailed seasonal
175 variability, enabling the model to work in environments with more complex interaction between $\delta^{18}\text{O}_w$
176 and temperature on the $\delta^{18}\text{O}_c$ record (see **equations 1 and 2**). This $\delta^{18}\text{O}_w$ data can be provided either
177 as a vector (with the same length as the data) or a single value (assuming constant $\delta^{18}\text{O}_w$) through the
178 $d18\text{O}_w$ parameter in the `run_model` function.

Formatted: Not Superscript/ Subscript

Formatted: Not Superscript/ Subscript

$$T[^{\circ}\text{C}] = T_{av} + \frac{T_{amp}}{2} \sin\left(\frac{2\pi * \left(t[d] - T_{pha} + \frac{T_{per}}{4}\right)}{T_{per}}\right) \quad (4)$$

181

Table 1: Overview of model parameters

Name	Description	Unit	Range
T_{av}	Average temperature	°C	Variable, generally between 0°C–30°C
T_{amp}	Temperature range (2*amplitude)	°C	Variable, generally <20°C
T_{pha}	Phase of temperature sinusoid	d	0–365 days
T_{per}	Period of temperature sinusoid	d	365 days by default
G_{av}	Average growth rate	$\mu\text{mm/d}$	Variable, generally between 0–100 $\mu\text{mm/day}$
G_{amp}	Range of growth rates	$\mu\text{mm/d}$	Variable, generally <200 $\mu\text{mm/day}$
G_{pha}	Phase of growth rate sinusoid	d	0–365 days
G_{per}	Period of growth rate sinusoid	d	365 days by default
G_{skw}	Skewness factor of GR sinusoid	-	0–100, with 50 meaning no skew
D	Depth-Distance along the record	μmm	Depends on archive
t	Age	d	Depends on archive
L_{win}	Length of sampling window	#	Depends on sampling resolution
w	Weighing factor on sample	-	0–1
i	Position relative to model window	-	0– L_i
I	Intercept of sinusoid (T_{av} or G_{av})		
A	Amplitude of sinusoid $\left(\frac{T_{amp}}{2} \text{ or } \frac{G_{amp}}{2}\right)$		
P	Period of sinusoid (T_{per} or G_{per})	d	
φ	Phase of sinusoid (T_{pha} or G_{pha})	d	

182

183 If marine $\delta^{18}\text{O}_c$ records represent one extreme on the spectrum of temperature versus $\delta^{18}\text{O}_w$ influence
184 on the $\delta^{18}\text{O}_c$ record, cave environments, in which $\delta^{18}\text{O}_c$ variability is predominantly driven by $\delta^{18}\text{O}_w$
185 variability in the precipitation fluid, represent the other extreme (Van Rampelbergh et al., 2014). In its
186 current form, ShellChron takes $\delta^{18}\text{O}_w$ as a user-supplied parameter to model temperature and growth
187 rate variability, but future versions will allow temperature to be fixed, while $\delta^{18}\text{O}_w$ becomes the modelled
188 variable. ShellChron's modular character makes it possible to implement this update without changing
189 the structure of the model. Application of ShellChron on $\delta^{18}\text{O}_c$ records from cave deposits will have to
190 be treated with caution, since drip water $\delta^{18}\text{O}_w$ seasonality (if present) cannot always be approximated
191 by a sinusoidal function and equilibrium fractionation in cave deposits is less common than in bio-
192 archives (Baldini et al., 2008; Daëron et al., 2011; Van Rampelbergh et al., 2014).

193 Besides temperature (or $\delta^{18}\text{O}_w$) seasonality, ShellChron models the growth rate of the archive to
194 approximate the $\delta^{18}\text{O}_c$ record (see [equation 5](#) and [Table 1](#), and [SI4](#); [growth_rate_curve](#) function;
195 visualized in [Fig. 4B](#) and [Fig S2](#)). Since the growth rate of many carbonate archives varies seasonally,
196 a quasi-sinusoidal model for growth rate seems plausible (e.g. Le Tissier et al., 1994; Baldini et al.,
197 2008; Judd et al., 2018). However, as discussed in Judd et al. (2018), the occurrence of growth

Formatted: Font: Not Bold

206 cessations (growth rate = 0) and skewness in seasonal growth patterns calls for a more complex growth
 207 rate model that can take these properties into account. Therefore, ShellChron uses a slightly modified
 208 version of the skewed sinusoidal growth function described by Judd et al. (2018; **equation 5**). Note that
 209 the added complexity of this function does not preclude the modelling of growth rate functions described
 210 by a simple sinusoid (no skewness; $G_{skw} = 50$) or even constant growth through the year ($G_{amp} = 0$; see
 211 **Table 1**).

$$212 \quad G[mm/yr] = G_{av} + \frac{G_{amp}}{2} \sin\left(\frac{2\pi * (t[d] - G_{pha} + G_{per} * S)}{P}\right)$$

$$213 \quad \text{with } S = \begin{cases} \frac{100 - G_{skw}}{50}, & \text{if } t[d] - G_{pha} < G_{per} \frac{100 - G_{skw}}{100} \\ \frac{G_{skw}}{50}, & \text{if } t[d] - G_{pha} \geq G_{per} \frac{100 - G_{skw}}{100} \end{cases} \quad (5)$$

214 Contrary to previous $\delta^{18}O_c$ growth models, ShellChron allows uncertainties on the input variables (**depth**
 215 **sampling distance** and $\delta^{18}O_c$ measurements) as well as uncertainties of the full modelling approach to
 216 be propagated, providing confidence envelopes around the chronology. Uncertainty propagation is
 217 optional and can be skipped without compromising model accuracy. Standard deviations of uncertainties
 218 on input variables (**depth-sampling distance** and $\delta^{18}O_c$) can be provided by the user, while model
 219 uncertainties are calculated from the variability in model results of the same datapoint obtained from
 220 overlapping simulation windows (see *growth_model* function). Measurement errors are combined by
 221 projecting Monte Carlo simulated values for **depth-sampling distance** and $\delta^{18}O_c$ measurements on the
 222 modelled $\delta^{18}O_c$ curve through an orthogonal projection (**equation 6**; *mc_err_orth* function; visualized in
 223 **Fig S3**). The measurement uncertainty projected on the **depth-distance** domain is then combined with
 224 the model uncertainty to obtain pooled uncertainties in the **depth-distance** domain, which are propagated
 through the modelled $\delta^{18}O_c$ record to obtain uncertainties on the model result in the age domain. As a
 result of the sliding window approach in ShellChron, model results for datapoints situated at the edges
 of windows are more sensitive to small changes in the modelled parameters and therefore possess a
 larger model uncertainty. To prevent these **less-least** certain model estimates from affecting the stability
 of the model, model results **were-are** given more weight the closer they **were-are** situated towards the
 center of the model window (see **equation 7** in *export_results* function; see also **Fig. S4**). This weighing
 is also incorporated in uncertainty propagation through a weighted standard deviation (see **equation 8**
 from the *sd_wt* function).

225

$$\sigma_{meas} = \sqrt{\left(\frac{D_{sim} - \overline{D_{sim}}}{\sigma_D}\right)^2 + \left(\frac{\delta^{18}O_{sim} - \overline{\delta^{18}O_{sim}}}{\sigma_{\delta^{18}O}}\right)^2} \quad (6)$$

226

$$w[i] = 1 - \left| \frac{2i}{L_{window}} - 1 \right| \quad (7)$$

227

$$\sigma_{weighted,i} = \sqrt{\frac{w_i * (x_i - \bar{w})^2}{\sum w[i] * \frac{N-1}{N}}} \quad (8)$$

228

229 3. Model description

230 ShellChron is organized in a series of functions that describe the step-by-step modelling process. A
 231 schematic overview of the model is given in **Fig. 1**. A short Test Case is used to illustrate the modelling
 232 steps in ShellChron. Fig. 2 shows how the virtual Test Case was created from randomly generated
 233 seasonal growth rate, $\delta^{18}O_w$ and temperature curves using the *seasonalclumped* R package (de Winter
 234 et al., 2021; see Fig. 2, Supplementary Methods and SI2) A wrapper function (*wrap_function*) is
 235 included which carries out all steps of the model procedure in succession to promote ease of use.

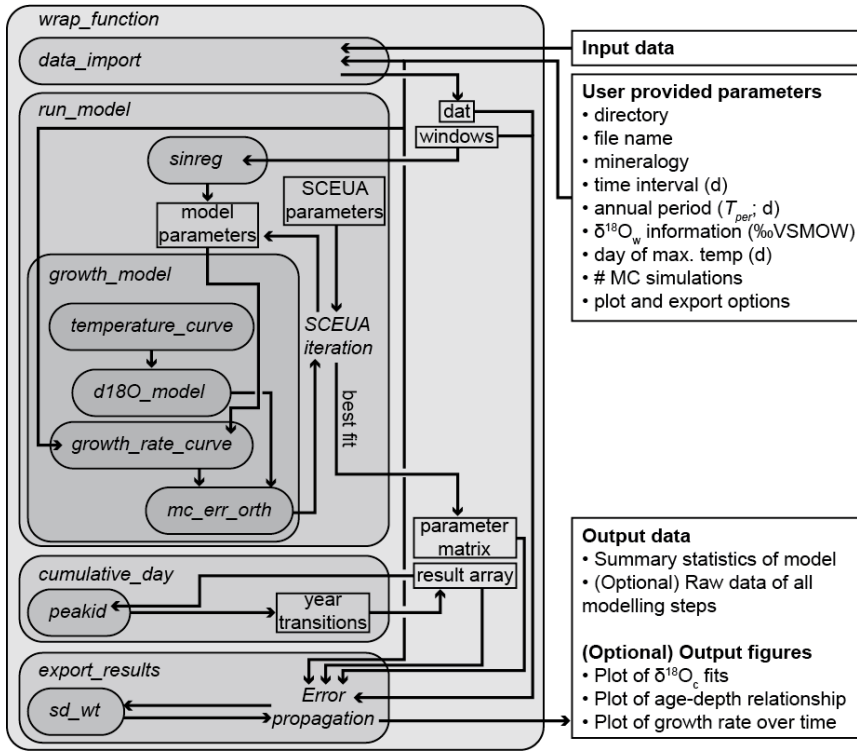
236

Formatted: Font: Bold

Formatted: Font: Bold

Formatted: Font: Not Bold

Schematic overview of ShellChron model



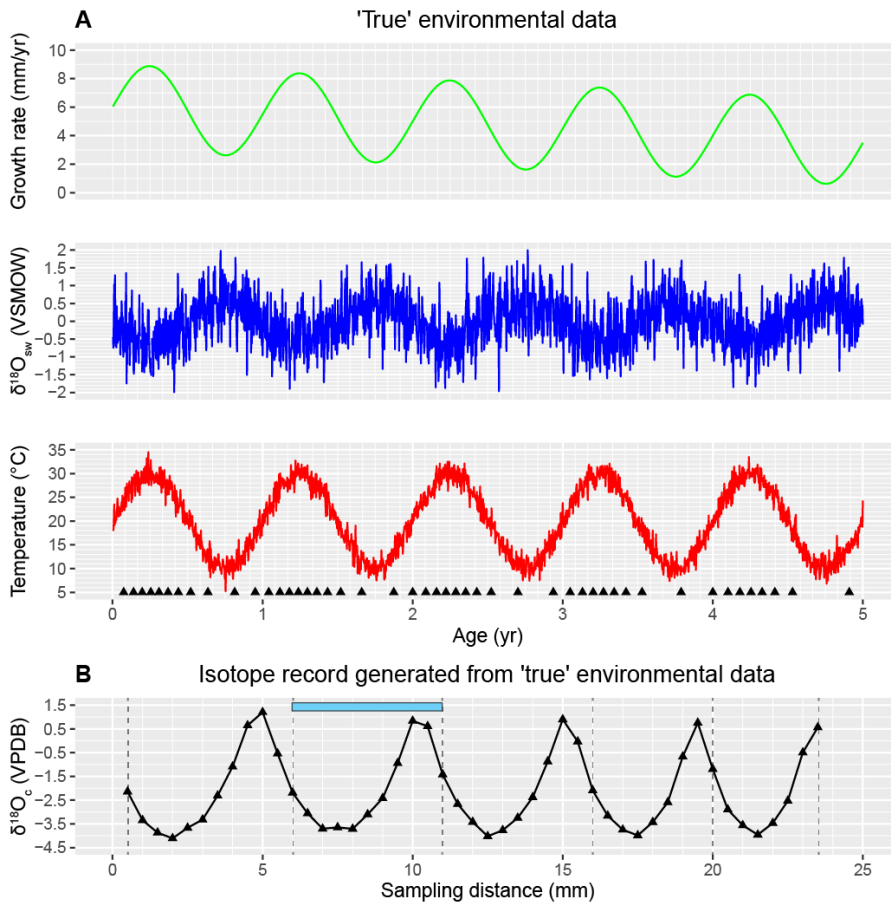
237

238 **Figure 1:** Schematic overview of ShellChron. Names in *italics* refer to functions (encapsulated in
 239 rounded rectangular boxes) and operations within functions. Rectangular boxes represent data. Arrows
 240 represent the flow of information between model components. Note that some operations are
 241 encapsulated in functions (e.g. *Error propagation* in *export results*) and that some functions are only
 242 used within other functions (e.g. *peakid* in *cumulative_day*). All data structures outside *wrap_function*
 243 represent input and output of the model. Detailed documentation of all functions and operations in
 244 ShellChron is provided in **SI1** ([see also Code availability](#)).

245

Formatted: Font: Not Bold

Formatted: Font: Not Bold



246

247

248

249

250

251

252

253

254

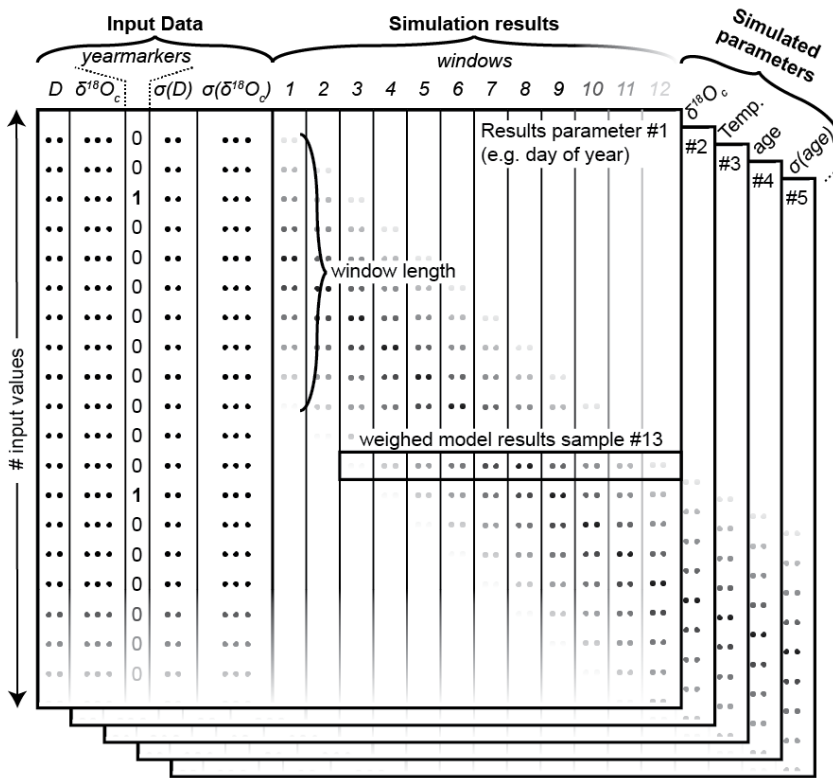
Figure 2: **A)** Plots of the growth rate (light green), $\delta^{18}\text{O}_w$ (blue) and Temperature (red) records (in time domain) from which the **Test case** was produced. Black triangles on the bottom of the temperature plot indicate the ages of the samples taken from the record. **B)** The $\delta^{18}\text{O}_c$ record for the **Test Case** generated after equidistant sampling using the *seasonalclumped* package (de Winter et al., 2021) with a sampling interval of 0.5 mm. Error bars on sampling distance (0.1 mm) and $\delta^{18}\text{O}_c$ (0.1‰) fall within the symbols. Vertical grey dashed lines indicate user-provided year markers and the blue bar on top of this plot shows an example of the width of a modelling window. See **Supplementary Methods** for details on producing the **Test case** $\delta^{18}\text{O}_c$ record and **SI3** for the R script used to generate the data.

Formatted: Line spacing: Double

255 Data is imported through the `data_import` function, which takes a comma-separated text file (CSV) with
256 the input data. Data files need to contain columns containing `depth_sampling_distance` (D , in μm) and
257 $\delta^{18}\text{O}_c$ data (in ‰VPDB), a column marking years in the record (`yearmarkers`) and two optional columns
258 containing uncertainties on `depth_sampling_distance` ($\sigma(D)$, one standard deviation, in μm) and $\delta^{18}\text{O}_c$
259 ($\sigma(\delta^{18}\text{O}_c)$, one standard deviation, in ‰) respectively (see example in **SI2** and **Figure 32**). The function
260 uses the year markers (third column) as guidelines for defining the minimum length of the model
261 windows to ensure that all windows contain at least one year of growth. Window sizes are defined to
262 contain at least two year markers (see Fig. 2). -By default, consecutive windows are shifted by one
263 datapoint, yielding a total number of windows equal to the sample size minus the length of the last
264 window. While year markers are required for ShellChron to run (otherwise no windows can be defined),
265 the result of the model does not otherwise depend on user-provided year markers, instead basing the
266 age result purely on simulations of the $\delta^{18}\text{O}_c$ data.

267

Schematic overview of result array structure

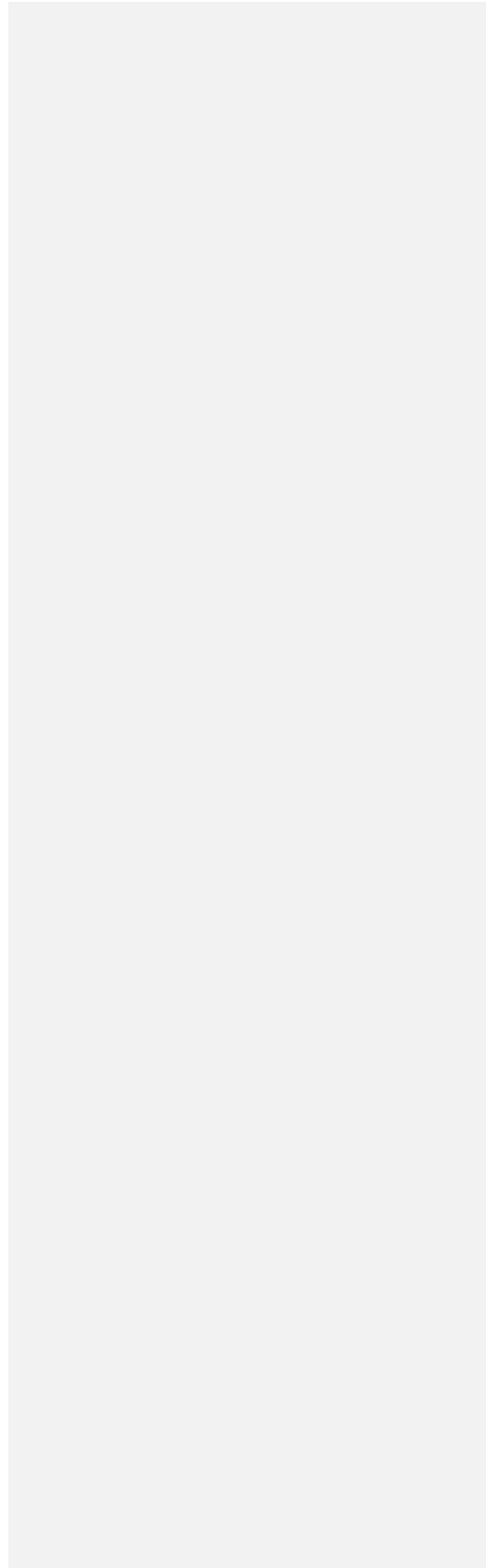


268

269 **Figure 32:** Schematic overview of the structure of the result array in which ShellChron stores the raw
 270 results of each model window. Data is stored in three dimensions: The sample number (rows in the
 271 figure), the window number (columns in the figure) and the number of modelled parameters (represented
 272 by the stacked table "sheets" in the figure). Note that the first 5 columns of each "sheet" represent the
 273 user-provided input data (see example in **SI2**), and that the model result data starts from column 6. The
 274 window length is determined by the user-provided indication of year transitions (column 3). Rows of dots
 275 in the figure are placeholders for (input or result) values. Shading of these dots in the window columns
 276 indicate differential weighing of modelled values in function of their location relative to the sliding window.
 277 The horizontal box shows how these weighing factors within each sample window (in vertical direction)
 278 result in weighing of different estimates of modelled parameters for the same data point (in horizontal
 279 direction). Shading of input data and window number towards the bottom and right edge of the figure,
 280 respectively, indicates that the number of input values (and thus simulation windows) is only limited to

281 the length of the input table and may therefore continue indefinitely (at the expense of longer
282 computation times, see [Figure-Fig. 85](#) in **Model performance**).

283



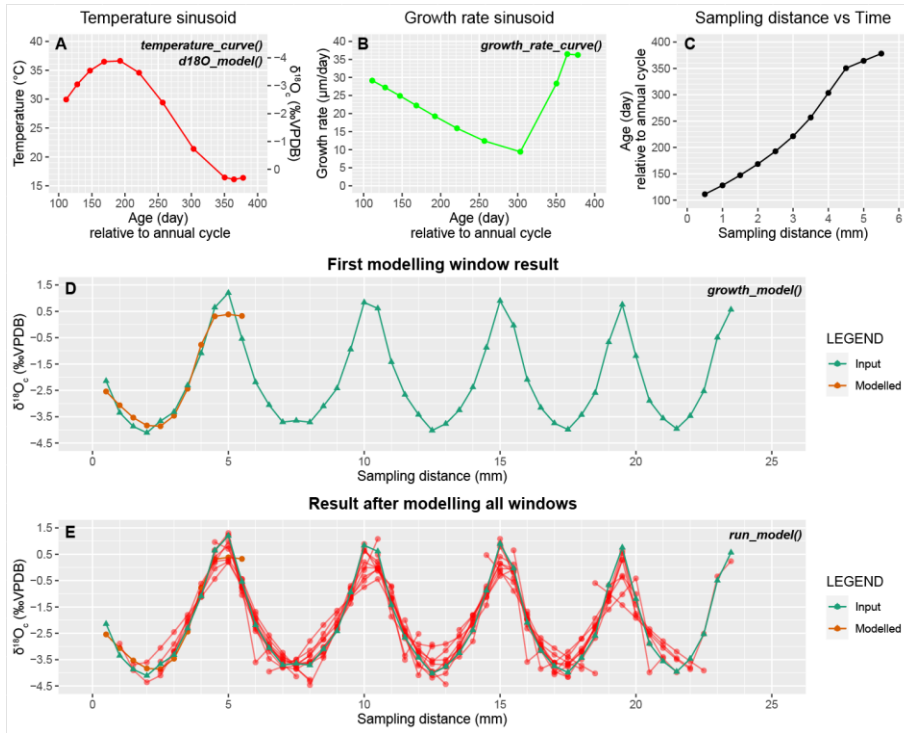
285 The core of the model consists of simulations of overlapping subsamples (windows) of the **depth**
286 **sampling distance** and $\delta^{18}\text{O}_c$ data described by the *run_model* function (see **Fig. 1 and 23**). Data and
287 window sizes are passed from *data_import* onto *run_model* along with user-provided parameters (e.g.
288 $\delta^{18}\text{O}_w$ information; see **Fig. 1**). *run_model* loops through the data windows and calls the *growth_model*
289 function, which fits a modelled $\delta^{18}\text{O}_c$ vs. **depth-distance** curve through the data using the SCEUA
290 optimization algorithm (see Duan et al., 1992; [see example in Fig 4](#)). The simulated $\delta^{18}\text{O}_c$ curve is
291 produced through a combination of a temperature sinusoid (*temperature_curve* function; see **equation**
292 **4, Fig. 4A** and **Fig. S1**) and a skewed growth rate sinusoid (*growth_rate_curve*; see **equation 5, Fig.**
293 **4B** and **Fig. S2**), with temperature data converted to $\delta^{18}\text{O}_c$ data through the *d18O_model* function
294 (**equation 1 and 2, Fig. 4A**).

295

Formatted: Font: Not Bold

Formatted: Font: Not Bold

Formatted: Font: Not Bold



296
 297 **Figure 4:** Showing the steps taken to simulate $\delta^{18}\text{O}_c$ data in the `run_model()` function on the **Test case**.
 298 **A)** Temperature sinusoid used to approximate $\delta^{18}\text{O}_c$ data in the first modelling window (see **D**), produced
 299 using a combination of `temperature_curve` and `d18O_model()` functions. Symbols indicate the positions
 300 of $\delta^{18}\text{O}_c$ samples on the temperature curve, with estimated $\delta^{18}\text{O}_c$ values shown on the secondary axis
 301 (right). **B)** Skewed growth rate sinusoid fit to the $\delta^{18}\text{O}_c$ data using the `growth_rate_curve` function. Note
 302 the shift towards steeper growth rate increase around the 300th model day (autumn season in this
 303 example). See **Fig. S2** for a detailed description of the growth rate sinusoid. **C)** The modelled age-
 304 distance relationship for this window after fitting $\delta^{18}\text{O}_c$ data, resulting from aligning the estimated age of
 305 samples (x-axes on **A**) with the distance in sampling direction (x-axis in **D**) using the cumulative growth
 306 rate function (**B**). **D)** $\delta^{18}\text{O}_c$ profile of the **Test case** (green) with the $\delta^{18}\text{O}_c$ curve of the first modelling
 307 window (red), which results from the combination of temperature (**A**) and growth rate (**B**) sinusoids,
 308 plotted on top (`growth_model` function). **E)** Result after simulating the full $\delta^{18}\text{O}_c$ profile of the **Test case**
 309 (green) using `run_model`, with the $\delta^{18}\text{O}_c$ curves of individual modelling windows shown in red.

Formatted: Justified, Line spacing: Double

Formatted: Font: Not Bold

Formatted: Font: Not Bold

Formatted: Superscript

310 -By default, starting values for the parameters describing temperature and growth rate curves are
311 obtained by estimating the annual period (P) through a spectral density estimation and applying a
312 linearized sinusoidal regression through the $\delta^{18}\text{O}_c$ data (*sinreg* function; see **equation 9**). It is possible
313 to skip this sinusoidal modelling step through the "*sinfit*" parameter in the *run_model* function, in which
314 case the starting value for the annual period is set equal to the width of the model window. In addition,
315 *growth_model* takes a series of ~~fixed~~ parameters describing the method for SCEUA optimization (see
316 Duan et al., 1992; Judd et al., 2018) and the upper and lower bounds for parameters describing
317 temperature and growth rate curves (see **S13S14**). Parameters for the SCEUA algorithm (*iniflg*, *ngs*,
318 *maxn*, *kstop*, *pcento* and *peps*) in the *run_model* function may be modified by the user to reach more
319 desirable optimization outcomes. The effect of changing the SCEUA parameters on the model result for
320 the Test case is illustrated in section 4.1, (see Fig. 5). If uncertainties on ~~depth-sampling distance~~ and
321 $\delta^{18}\text{O}_c$ data are provided, *growth_model* calls the *mc_err_orth* function to propagate these errors through
322 the model result (see **equation 6** and **Fig S3**).

Formatted: Font: Not Italic

Formatted: Font: Not Bold

Formatted: Font: Not Bold

$$323 \quad \delta^{18}\text{O}_c[\text{‰VPDB}] = I + \frac{A}{2} \sin\left(\frac{2\pi * (D - \varphi + \frac{P}{4})}{P}\right),$$

$$324 \quad \text{linearized as: } \delta^{18}\text{O}_c[\text{‰VPDB}] = a + b \sin\left(\frac{2\pi}{P} * D\right) + c \cos\left(\frac{2\pi}{P} * D\right),$$

$$325 \quad \text{with } I = a; A = \sqrt{b^2 + c^2} \text{ and } \varphi = P * \left(0.25 - \frac{\cos^{-1}\left(\frac{b}{A}\right)}{2\pi}\right) \quad (9)$$

326 The *run_model* function returns an array listing day of the year (1–365), temperature, $\delta^{18}\text{O}_c$, growth rate
327 and (optionally) their uncertainty standard deviations as propagated from uncertainties on the input data
328 ("result array"; see **Fig. 32** and **S14S15**). Note that the default length of the year (*Tper* and *Gper*) is set
329 at 365 days, but that these parameters can be modified by the user in *run_model*. In addition, a matrix
330 containing the optimized parameters of temperature and growth rate curves is provided, yielding
331 information about the evolution of mean values, phases, amplitudes, and skewness of seasonality in
332 temperature and growth rate along the record ("parameter matrix", see **Fig. 1** and **S15S16**). To construct
333 an age model for the entire record, the modelled timing of growth data, expressed as day relative to the
334 365-day year, ~~needs to be~~ converted into a cumulative time series listing the number of days relative
335 to the start of the first year represented in the record (rather than relative to the start of the year in which

336 the datapoint is found). This requires year transitions (transitions from day 365 to day 1) to be recognized
337 in all the model results. The *cumulative_day* function achieves this by aggregating information about
338 places where the beginning and end of the year is recorded in individual window simulations and
339 applying a peak identification algorithm (*peakid* function) to find places in the record where year
340 transitions occur (see **Supplementary Methods**). Results of the timing of growth for each sample (in
341 day of the year) are converted to a cumulative time scale using their positions relative to these
342 recognized year transitions (**Supplementary Methods**).

343 In a final step (described by the *export_results* function), the results from overlapping individual
344 modelling windows are combined to obtain mean values and 95% confidence envelopes of the result
345 variables (age, $\delta^{18}\text{O}_c$, $\delta^{18}\text{O}_c$ -based temperatures and growth rates) for each sample in the input data. If
346 uncertainties on the input variables were provided, these are combined with uncertainties on the
347 modelling result calculated from results of the same datapoint on overlapping data windows by pooling
348 the variance of the uncertainties (**equation 10**). Throughout this merging of data from overlapping
349 windows, results from datapoints on the edge of windows are given less weight than those from
350 datapoints near the center of a window (see **equation 7** and **Fig. S4**). This weighing procedure corrects
351 for the fact that datapoints near the edge of a window are more susceptible to small changes in the
352 model parameters and are therefore less reliable than results in the center of the window. Finally,
353 summaries of the simulation results and the model parameters including their confidence intervals are
354 exported as comma-separated (CSV) files. In addition, *export_results* supports optional exports of
355 figures displaying the model results and files containing raw data of all individual model windows
356 (equivalent to "sheets" of the result array, see **Fig. 23** and **SI4SI5**).

$$VAR_{pooled} = \frac{\sum_i ((N_i - 1) * VAR_i * w_i)}{\sum_i (N_i) - n} \quad (10)$$

357
358 in which w = weight of the individual reconstructions, N is the sample size and n is the number of
359 reconstructions (indexed by i) that is combined ~~(10)~~

360

Formatted: Centered

361 **4. Model performance**

362 The performance of ShellChron was first tested on two-three virtual datasets:

- 363 1. The short **Test case** used to illustrate the model steps above (see **Fig. 2** and **4; SI7**)
- 364 2. A $\delta^{18}\text{O}_c$ record constructed from a simulated temperature sinusoid with added stochastic noise
365 (**Case 1; SI6SI8**) and one
- 366 3. A **record** based on a real high-resolution sea surface temperature and salinity record measured
367 on the coast of Texel island in the tidal basin of the Wadden Sea ~~in the north of the (North~~
368 Netherlands ~~(; Texel~~, see details in **SI7–SI9** and de Winter et al., ~~2020d~~**2021**, and
369 **Supplementary Methods**).

370 Firstly, the effect of varying parameters in the SCEUA algorithm is tested on the **Test Case (Fig. 5)**.

371 Then, full model runs on **Case 1** and **Texel** are evaluated in terms of model performance (**Fig. 6**).

372 In addition to the three test cases, three modern carbonate $\delta^{18}\text{O}_c$ records were internally dated using
373 ShellChron (see **Fig. 7**): a tropical stony coral (*Porites lutea*; hereafter: **coral**) from the Pandora
374 Reef (Great barrier Reef, NE Australia; Gagan et al., 1993; see **SI8SI10**), a Pacific oyster shell
375 (*Crassostrea gigas*; hereafter: **oyster**) from List Basin in Denmark (Ullmann et al., 2010; see
376 **SI8SI10**) and a temperate zone speleothem from Han-sur-Lesse cave (Belgium; hereafter:
377 **speleothem**; see Vansteenberghe et al., 2019; see **SI8SI10**). Finally, ShellChron's performance in
378 terms of computation time and accuracy is compared to that of the most comprehensive pre-existing
379 $\delta^{18}\text{O}_c$ -based age model (by Judd et al., 2018) on simulated temperature sinusoids of various length
380 and sampling resolutions to which stochastic noise was added (*sensu* **Case 1**; de Winter et al.,
381 ~~2020d~~**2021**; see **Fig. 8** and **SI119**). The latter also demonstrates the scalability of ShellChron and
382 its application on a variety of datasets. Timing comparisons were carried out using a modern laptop
383 (Dell XPS13–7390; Dell Inc., Round Rock, Tx, USA) with an Intel Core i7 processor (8 MB cache,
384 4.1 GHz clock speed, 4 cores, Intel Corporation, Santa Clara, CA, USA), 16 GB LPDDR3 RAM and
385 a SSD drive running Windows 10. Note that ShellChron was built and tested successfully on Mac
386 OS, Fedora Linux and Ubuntu Linux as well.

Formatted: Font: (Default) Arial, 10 pt

Formatted: Font: Not Bold

Formatted: Font: Not Bold

Formatted: Font: (Default) Arial, 10 pt

Formatted: Font: (Default) Arial, 10 pt

Formatted: Font: (Default) Arial, 10 pt

Formatted: Font: (Default) Arial, 10 pt

Formatted: Font: (Default) Arial, 10 pt

Formatted: Font: (Default) Arial, 10 pt

Formatted: Font: (Default) Arial, 10 pt

Formatted: Font: (Default) Arial, 10 pt

Formatted: Indent: Left: 0.25"

Formatted: Font: Bold

Formatted: Font: (Default) Arial, 10 pt

Formatted: Font: (Default) Arial, 10 pt

Formatted: Font: (Default) Arial, 10 pt

Formatted: Font: (Default) Arial, 10 pt

Formatted: Font: (Default) Arial, 10 pt

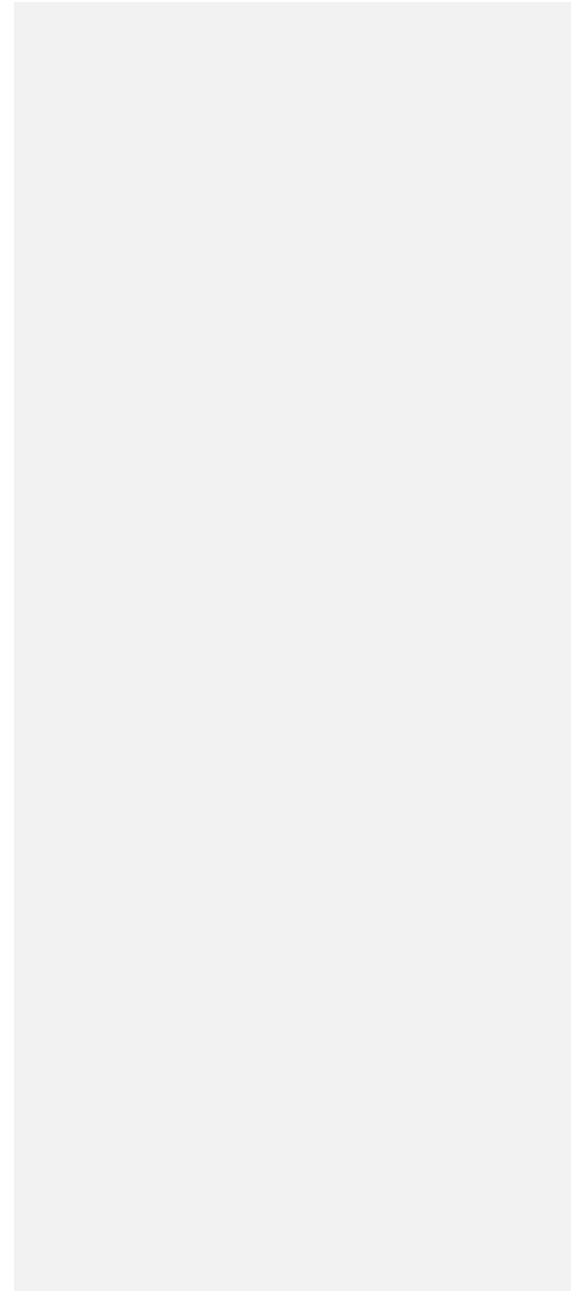
Formatted: Font: (Default) Arial, 10 pt

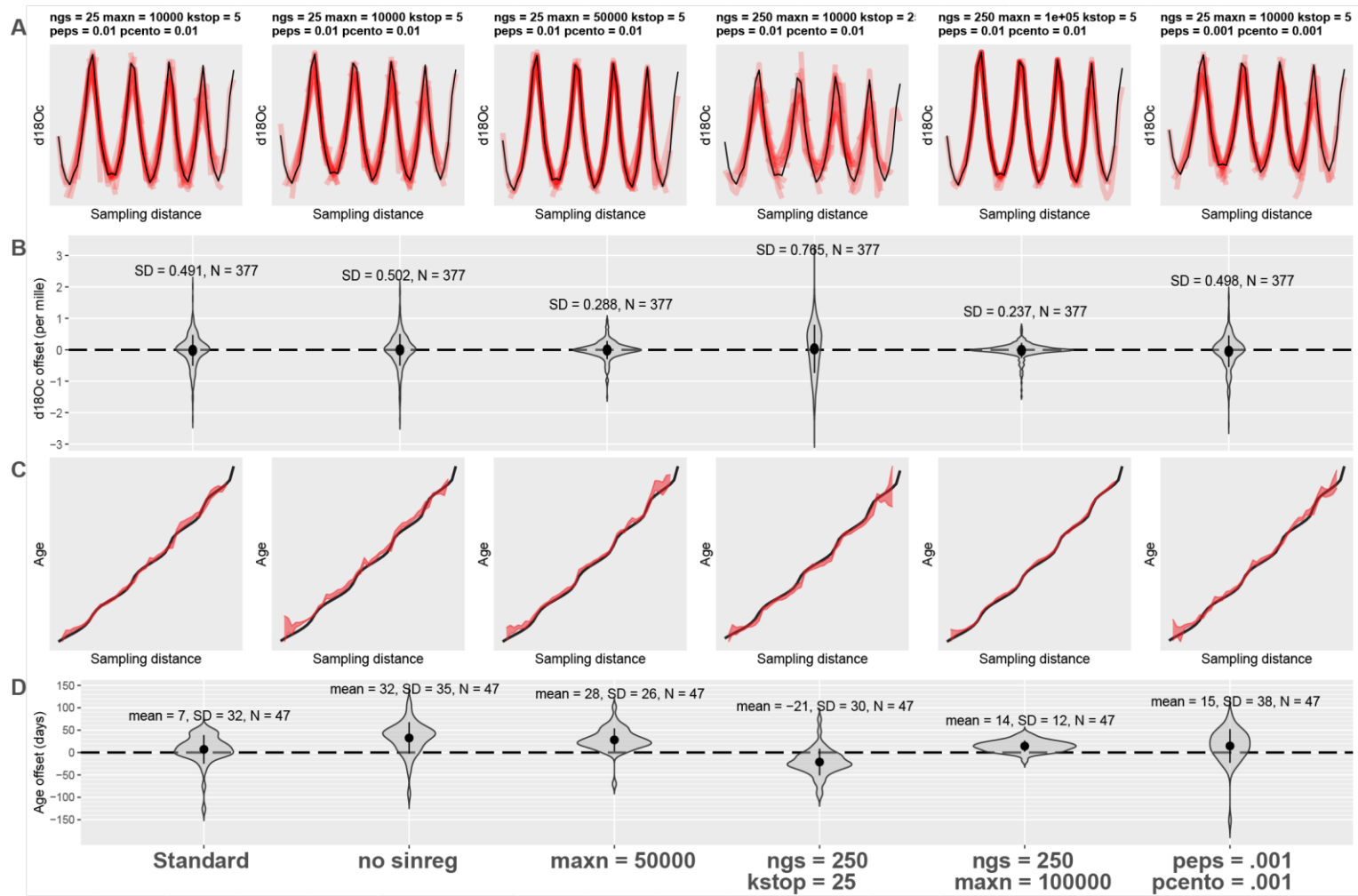
Formatted: Font: (Default) Arial, 10 pt

Formatted: Font: (Default) Arial, 10 pt

Formatted: Font: (Default) Arial, 10 pt

387
388





390 **Figure 5;** Result of testing ShellChron with various combinations of SCEUA parameters and
391 sinusoidal regression on the **Test case** dataset (see **Fig. 2**). The leftmost plots illustrate performance
392 of ShellChron under default SCEUA parameters. Plots to the right show various combinations of
393 parameters that deviate from the default (see labels on top and bottom of plot **A**) Fits of the model
394 $\delta^{18}\text{O}_e$ curves (red) with the data (black). **B**) Violin plots showing the distribution of modelled $\delta^{18}\text{O}_e$
395 offset from the data. **C**) Age-distance plots showing modelled (red) and true (black) age-depth
396 relationships for each scenario. **D**) Violin plots showing the distribution of age offsets from the real
397 age-depth relationship. SD = standard deviation, N = number of datapoints, sinres = sinusoidal
398 regression, maxn, ngs, kstop, peps and pcento are SCEUA parameters (see Duan et al., 1992 and
399 explanation in **section 4.1**). Data on test results is provided in **SI11**.

400 **4.1 Testing model parameters**

401 Testing different combinations of modelling parameters (**Fig. 5**) shows that, while the results of
402 ShellChron can improve beyond the default SCEUA parameters and sinusoidal regression, care must
403 be taken to evaluate the effect of changing modelling parameters on both the $\delta^{18}\text{O}_e$ fit and the age-
404 distance relationship. Comparative testing on the **Test case (Fig. 5)** shows that sinusoidal regression
405 has a negligible influence on the success of ShellChron fitting the $\delta^{18}\text{O}_e$ curve (**Fig. 5A-B**; standard
406 deviation on $\delta^{18}\text{O}_e$ is 0.49‰ with sinusoidal regression and 0.50‰ without). However, ShellChron with
407 sinusoidal regression performs better in terms of age approximation, with a mean age offset of only 7
408 ± 32 days with sinusoidal regression against 32 ± 35 days without (**Fig. 5C-D**). Age-distance plots
409 (**Fig. 5C**) show that the model without sinusoidal fit shows a phase offset with respect to the real age-
410 depth relationship, resulting in overestimation of the age for much of the record. Sinusoidal regression
411 probably results in better initial parameter estimation, which helps to avoid phase offsets like the one
412 shown in **Fig. 5**. For the remainder of the tests, sinusoidal regression was used.

413 The remainder of the tests show that the main bottleneck towards better $\delta^{18}\text{O}_e$ fit optimization is the
414 maximum number of function evaluations allowed within a single modelling cycle (maxn; see **Fig. 5**).
415 Increasing the other SCEUA parameters, such as the number of complexes in the SCEUA routine
416 (ngs), the number of shuffling loops that should show a significant change before convergence (kstop)
417 and the thresholds for significant change in parameter value (peps) or result value (pcento) does not
418 improve the result if the SCEUA algorithm is not allowed more processing time (maxn). In fact, **Fig. 5**

Formatted: Line spacing: Double

Formatted: Font: Not Bold

Formatted: Font: Not Bold

Formatted: Font: Not Italic

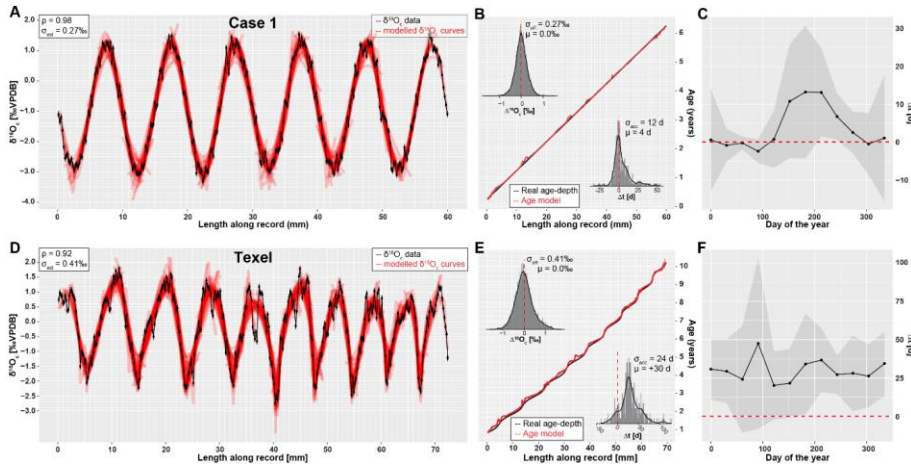
419 shows that increasing these SCEUA parameters can actually result in a worse $\delta^{18}\text{O}_c$ fit and higher
420 uncertainty on the age result (Fig. 5B and D). A fivefold increase in maxn ($\text{maxn} = 50000$) almost
421 halves the standard deviation on $\delta^{18}\text{O}_c$ residuals (from 0.49‰ to 0.29‰; Fig. 5B) and decreases the
422 standard deviation on the age model offset from 32 to 26 days (Fig. 5D). A combination of a tenfold
423 increase in function evaluations with an equal multiplication of the number of complexes in the SCEUA
424 routine (ngs; see details in Duan et al., 1992) results in a further reduction of standard deviations on
425 $\delta^{18}\text{O}_c$ (0.23‰) and age result (12 days). These tests show that returns in terms of model precision
426 quickly diminish with increasing processing time. Since the total modelling time linearly scales with the
427 number of function evaluations, this tradeoff towards lower standard deviation on the modelling result
428 is costly. Since these function evaluations are repeated in each modelling window, the cost in terms of
429 extra processing time can increase quickly, especially for larger $\delta^{18}\text{O}_c$ datasets. In addition, in this
430 situation the mean model offset (accuracy of the model; 7 days, 28 days and 14 days for maxn of $1.0 \cdot$
431 10^4 , $5.0 \cdot 10^4$ and $1.0 \cdot 10^5$ respectively; Fig. 5D) does not significantly improve with increasing number
432 of function evaluations. Based on these results, the default maxn parameter in ShellChron was set to
433 10^4 to compromise between keeping modelling times short while retaining high model accuracy.
434 However, specific datasets may benefit from an increase in modeling time, so case-by-case
435 assessment of the optimal SCEUA parameters is recommended. A detailed evaluation of the total
436 modelling time in a typical $\delta^{18}\text{O}_c$ dataset is discussed in section 4.4.

Formatted: Font: Not Italic

Formatted: Font: Not Bold

437

438



439

440 **Figure 63:** Result of applying ShellChron on ~~the~~ two virtual datasets: **Case 1** (top, see [S16S18](#)) and
 441 **Texel**, (bottom, see [S17S19](#)). Leftmost panels (**A and D**) show the model fit of individual sample windows
 442 (red) on the data (black, including horizontal and vertical error bars), with in the top left Spearman's
 443 correlation coefficients (ρ) and standard deviations on the $\delta^{18}O_c$ estimate (σ_{est}). **Right-Middle** panels (**B**
 444 **and E**) show the resulting age model (red, including shaded 95% confidence level) compared with the
 445 real age-depth-distance relationship of both records. Histograms in the top left of age-depth-distance
 446 plots show the offset between modelled and measured $\delta^{18}O_c$ (as visualized in the-left panels **A and D**)
 447 with standard deviations of the $\delta^{18}O_c$ offset (σ_{off}) and offset averages (μ). Histograms in the bottom right
 448 of age-depth-distance plots show the offset between modelled and actual ages (in days) of each
 449 datapoint, including standard deviations on the age accuracy (σ_{acc}) and mean age offset (μ). **Note that**
 450 **the last 2 years' worth of data in the Texel dataset (shaded in yellow) show a positive offset of almost 1**
 451 **year due to an aberration in the data around 60 mm (see discussion in text)** Rightmost panels (**C and F**)
 452 **highlight age offset binned in monthly time bins to illustrate how accuracy varies over the seasons. Grey**
 453 **envelopes indicate 95% confidence levels on the monthly age offset.**

454

Formatted: Line spacing: Double

Formatted: Font: Bold

4.2 Artificial carbonate records

Results of running ShellChron on **Case 1** and **Texel** datasets (**Fig. 36**) show that modelled $\delta^{18}\text{O}_c$ records in individual windows closely match the data. A summary of ShellChron performance statistics is given in **Table 2**. In ~~both-all~~ virtual datasets, $\delta^{18}\text{O}_c$ estimates are equally distributed above and below the $\delta^{18}\text{O}_c$ data ($\overline{\Delta^{18}\text{O}_c} = 0.0 \text{ ‰}$; Spearman's ρ of ~~0.79-98~~ and ~~0.74-92~~ for **Case 1** and **Texel** datasets respectively). ~~Age offsets vary slightly over the seasons, but the difference between monthly time bins is not statistically significant on a 95% confidence level (Fig. 6C and F; and show no seasonal bias (see also S10S12) in both datasets.~~ The fact that ~~this is also the case for~~ seasonal bias in age offset is absent in the **Texel** dataset, which is skewed towards growth in the winter season and includes relatively strong seasonal variability in $\delta^{18}\text{O}_w$, shows that ShellChron is not sensitive to such subtle (though common) variability in growth rate or $\delta^{18}\text{O}_w$. In general, ShellChron's mean age assignment is accurate on a monthly scale (age offsets of ~~-194 ± 39-12~~ d and ~~+31-30 ± 128-24~~ d for **Case 1** and **Texel** datasets respectively). The sampling resolution in the **Texel** data contains some notable exceptions ~~decreases near the end of the record, where the sampling resolution is reduced (see S17S19), resulting in an overestimation of the age for data in the last two years in the record. On closer inspection, the inaccuracies result from a persistent reduction of $\delta^{18}\text{O}_c$ in the winter season around 60 mm along the record which is interpreted by the model as an extra annual cycle. This glitch results from the interplay of seasonally low $\delta^{18}\text{O}_w$ values and stochastic noise in high-resolution records and warrants a posteriori inspection of model results by the user. The offset in the last part of the record can be easily spotted by inspecting the growth curve and amended by subtracting the extra year from the affected datapoints. After correction, the accuracy of modelling the **Texel** age becomes (-22 ± 80 d) but this does not result in reduced age model accuracy. If anything, the age of **Texel** samples is better approximated near the end of the record, and age offsets are larger in the central part of the record (~30-50 mm; **Fig. 6E**). The lower accuracy in the third to fifth year of the **Texel** record is likely a result of the sub-annual variability in the record that is superimposed on the seasonal cycle. This variability is less pronounced near the end of the record, partly because this variability is not resolved at lower sampling resolution, which illustrates that higher sampling resolutions do not necessarily result in better age models.~~

Formatted: Font: Bold

Formatted: Font: Not Bold

Table 2: Overview of datasets and model results

Dataset	Resolution	Length	$\delta^{18}\text{O}_c$ seasonal range	Complications
<u>Test case</u>	<u>7-12 yr⁻¹</u>	<u>5 yr</u>	<u>~5‰</u>	<u>Variable $\delta^{18}\text{O}_w$, Variable GR</u>
Case 1	50 yr ⁻¹	6 yr	~4.3‰	None
Texel	26–45 yr ⁻¹	10 yr	~4‰	Variable $\delta^{18}\text{O}_w$, Variable GR
Coral	30–49 yr ⁻¹	6 yr	~1.7‰	Variable GR
Oyster	23–45 yr ⁻¹	3.5 yr	~3‰	Variable $\delta^{18}\text{O}_w$, Variable GR
Speleothem	4–13 yr ⁻¹	14 yr	~0.5‰	Variable $\delta^{18}\text{O}_w$, Variable GR, Non-sinusoidal $\delta^{18}\text{O}_c$ -forcing

Dataset	$\delta^{18}\text{O}_c$ offset ($\pm 1\sigma$)	Age offset ($\pm 1\sigma$)	Spearman's ρ	Observations
<u>Test case</u>	<u>0.0 \pm 0.49 ‰</u>	<u>7 \pm 32 d</u>	<u>0.94</u>	<u>Slightly out of phase</u>
Case 1	0.0 \pm 0.9127‰	-194 \pm 39-12 d	0.7998	-
Texel	0.0 \pm 0.7741‰	+3130 \pm 128-24 d (-21 \pm 80 d)	0.7192	Last 2 years off
Coral	0.0 \pm 0.1514‰	-2212 \pm 44-28 d	0.9697	-
Oyster	0.0 \pm 0.3539‰	-9-15 \pm 53-43 d	0.91	Reduced accuracy near growth stops
Speleothem	0.0 \pm 0.1308‰	105-114 \pm 166 59 d	0.7192	Susceptible to phase offsets: Only reliable on inter-annual scale

Formatted: Font: Not Bold

Formatted: Font: Not Bold

Formatted: Font: Not Bold

Formatted: Font: Not Bold

Formatted: Font: Not Bold

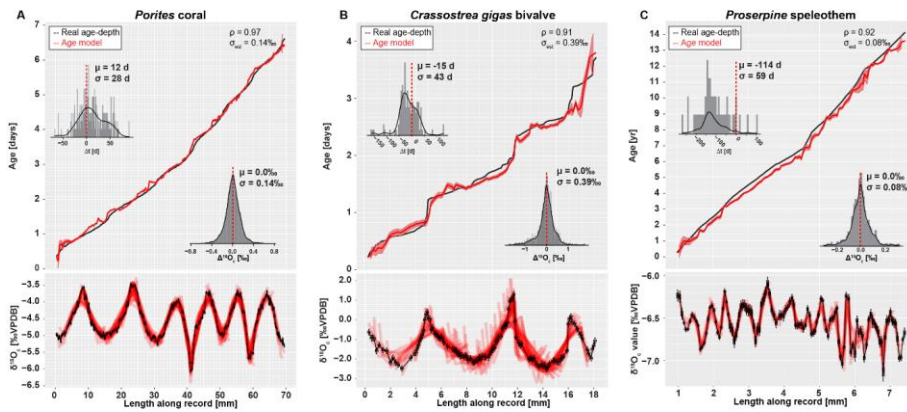
Formatted Table

Formatted: Font: Not Bold

Formatted: Font: Not Bold

Formatted: Font: Not Bold

Formatted: Font: Not Bold



484

485 **Figure 74:** Overview of model results for the three test datasets from real carbonate archives: **(A) coral**,
 486 **(B) oyster** and **(C) speleothem**. Lower panels indicate the fit of individual model windows (in red) with
 487 the data (in black) while upper panels show the age model (in red) compared to the “true” age-depth
 488 distance relationship with histograms showing model accuracy (in days, top left) and model fit ($\delta^{18}\text{O}$.
 489 offset in ‰, bottom right). Color scheme follows **Figure 3**. Note that the true age-depth-distance
 490 relationship is not known for these natural records, but is estimated using known growth seasonality
 491 (coral), comparison with *in situ* temperature and salinity measurements (oyster) or simply by
 492 interpolating between annual growth lines (speleothem). See **Supplementary Methods** for details [and](#)
 493 [S110](#) for raw data.-

494

4.3 Natural carbonate records

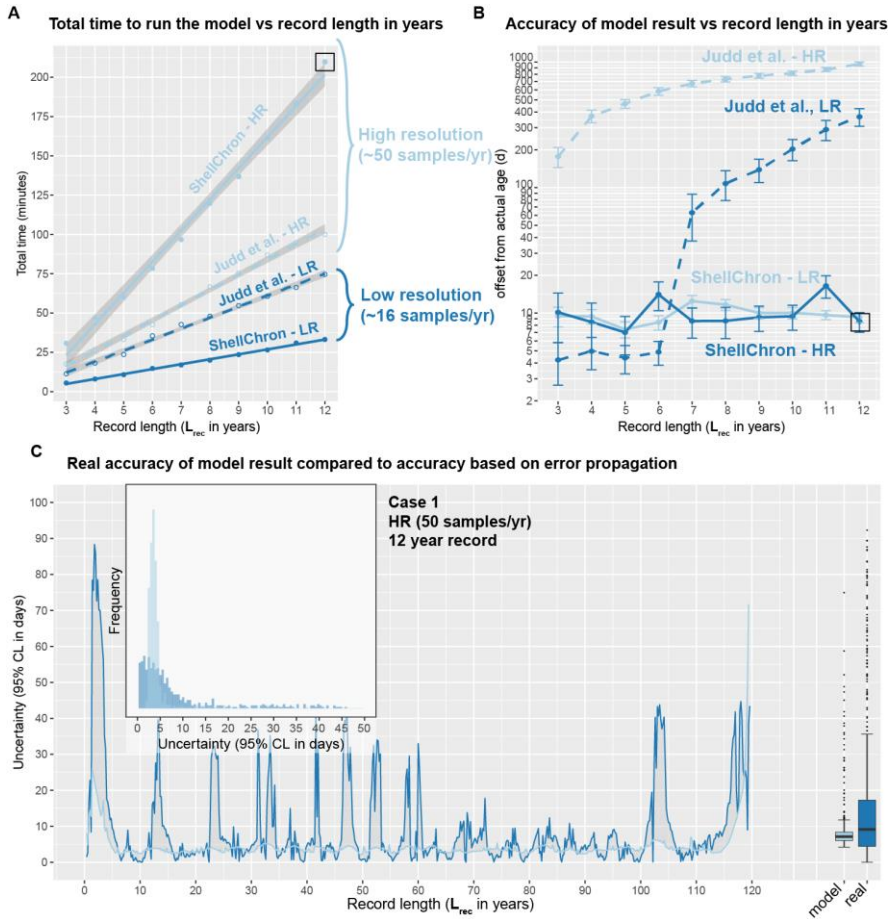
Formatted: Font: Bold

Results of modelling natural carbonate records (Fig. 4-7; and Table 2; see also S110) illustrate the effectiveness of ShellChron on different types of records. Performance clearly depends on the resolution of the record and the regularity of seasonal variability contained within. As in the virtual datasets, modelled $\delta^{18}\text{O}_c$ successfully mimic $\delta^{18}\text{O}_c$ data in all records ($\overline{\Delta^{18}\text{O}_c} = 0.0$; Spearman's ρ of 0.9697, 0.91 and 0.74-92 for coral, oyster and speleothem respectively). No consistent seasonal bias is observed in $\Delta^{18}\text{O}_c$ and model accuracy ($p > 0.05$; see Table 2 and S110-S112), despite significant (seasonal and inter-annual) variability contained in the records (especially in oyster and speleothem records). When comparing the accuracy of these records, it must be noted that the "real" age of the samples in these natural carbonates is not known with accuracy. Model results are instead compared with age models constructed using conventional techniques such as matching $\delta^{18}\text{O}_c$ profiles with local temperature and/or $\delta^{18}\text{O}_w$ variability (oyster and coral records) or even merely by linear interpolation between annual markers in the record (speleothem record; see Supplementary Methods). Despite this caveat, testing results clearly show that the least complicated record (coral; Fig. 4a7A), characterized by minimal variability in $\delta^{18}\text{O}_w$ and growth rate and a high sampling density, has the best overall model result ($\Delta^{18}\text{O}_c = 0.0 \pm 0.15-14$ compared to a $\sim 1.7\text{‰}$ seasonal range; $\rho = 0.9697$; $\Delta t = -2212 \pm 44-28$ d; see Table 2). The oyster record (Fig. 4b7B), which has strong seasonal variability in growth rate and $\delta^{18}\text{O}_{sw}$ also yields a very reliable age model ($\Delta^{18}\text{O}_c = 0.0 \pm 0.15-39$ compared to a $\sim 3\text{‰}$ seasonal range; $\rho = 0.91$; $\Delta t = -9-15 \pm 53-43$ d; see Table 2). The speleothem record (Fig. 4c7C), plagued by lower sampling resolution, large inter-annual $\delta^{18}\text{O}_c$ variability, restricted $\delta^{18}\text{O}_c$ seasonality and a lack of clearly seasonal $\delta^{18}\text{O}_c$ forcing, yields the least reliable model result ($\Delta^{18}\text{O}_c = 0.0 \pm 0.13-08$ compared to a $\sim 0.5\text{‰}$ seasonal range; $\rho = 0.7492$; $\Delta t = 405-114 \pm 466-59$ d; see Table 2). Note that the accuracy figure provided for the speleothem record is based on comparison with an age model based on linear interpolation between annual growth lines. This assumption of the age-distance relationship is almost certainly erroneous, since drip water supply to (and therefore growth in) has been shown to vary seasonally (e.g. Baldini et al., 2008), including at the very site the speleothem data derives from (Han-sur-Lesse cave, Belgium; Van Rampelbergh et al., 2014; Vansteenberge et al., 2019). However, since no reliable information is available on sub-annual variability in growth rates in this record, ShellChron results cannot be validated at the sub-annual scale in this case. The high age offset (-114 days) in the speleothem model result is a consequence of the assumption in ShellChron that the highest temperature (lowest

525 $\delta^{18}\text{O}_c$ value) recorded in each growth year happens halfway through the year (day 183). While this
526 assumption is approximately valid for temperature-controlled $\delta^{18}\text{O}_c$ records (see Fig. 6 and 7), it is
527 problematic for speleothems, in which $\delta^{18}\text{O}_c$ is often dominated by the $\delta^{18}\text{O}_w$ of drip water, which may
528 not be lowest during the summer season (see Van Rempelbergh et al., 2014). The timing of the $\delta^{18}\text{O}_c$
529 minimum can be set in the *run_model* function using the *t_maxtemp* parameter. Note that changing
530 *t_maxtemp* does not affect relative dating within the $\delta^{18}\text{O}_c$ record, but, if set correctly, results in a phase
531 shift of the age model result into better alignment with the seasonal cycle.

Formatted: Font: Not Bold

532



533

534 **Figure 85:** Overview of the result of timing ShellChron and the Judd et al. (2018) model on the same

535 datasets (A), comparing the accuracies of both models (B) and comparing the accuracy as calculated

536 by ShellChron with the real offset in the age model (C). In (A) and (B), low resolution datasets are plotted

537 in dark blue, while high-resolution datasets plot in redlight blue. Solid lines represent ShellChron and

538 dashed lines show performance of the Judd et al. model. The black box in (A) and (B) highlights the

539 dataset used in (C). In (C), grey-dark blue lines, bars and boxplot indicate true offset of the model from

540 the actual sample age, while red-light blue lines, bars and boxplot show the accuracy of the model as

541 calculated from the propagated errors on model and input data. Raw data is provided in S111.

4.4 Modeling time

Formatted: Font: Bold

The performance of both ShellChron and the Judd et al. model in terms of computation time linearly increases with the length of the record (in years; see **Fig. 58**, **Fig. S5** and **S19S11**). Computation time of ShellChron on the high-resolution test dataset (50 samples/yr) increases very steeply with the length of the record in years (~240 minutes per additional year), while the low-resolution dataset (16 samples/yr) shows a slower increase (~5.3 minutes per additional year; **Fig. 5A**). This contrasts with the model from Judd et al., which requires only slightly more time on high-resolution data than on low-resolution datasets (~7 and ~10 minutes per additional year, respectively). The difference is explained by the sliding window approach applied in ShellChron, which requires more SCEUA optimization runs per year in high-resolution datasets than in low resolution datasets. When plotted against the number of calculation windows or samples in the dataset, running ShellChron on low-resolution and high-resolution datasets require a similar increase in computation time (~0.4 minutes, or 24 seconds, per additional sample/window; **Fig. S5**) under default SCEUA conditions. ShellChron thus outcompetes the Judd et al. model in terms of computation time in datasets with fewer than ~20 samples per year, even though more SCEUA optimizations are required.

The key computational improvement in ShellChron is the application of a sinusoidal regression before each SCEUA optimization to estimate the initial values of the modelled parameters (*sinreg* function; see **equation 9** and **Fig. 1** in **Model description**). Since carbonate archives are rarely sampled for stable isotope measurements above 20 samples per year (e.g. Goodwin et al., 2003; Schöne et al., 2005; Lough, 2010 and references therein), the disadvantage of a steep computational increase for very high-resolution archives is, in practice, a favorable tradeoff for the added control on model and measurement uncertainty and smoother inter-year transitions ShellChron offers in comparison to previous models. The similarity of ShellChron's accuracy in the low- and high-resolution datasets demonstrates its robustness across datasets with various sampling resolutions (see also **Table 2** and **Fig. 4B7**).

Longer computation times in the Judd et al. model result in slightly better accuracy on the modelled age compared to ~~the present version of~~ ShellChron on the scale of individual datapoints in low-resolution datasets (see **Fig. 58B**). However, this advantage is rapidly lost when records containing multiple years are considered (**Fig. 5B8B**). The advantage of the ShellChron model is its application of overlapping model windows, which smooth out the transitions between modelled years and eliminate accumulations

571 of model inaccuracies when records grow longer. In addition, contrary to previous models, ShellChron
572 does not rely on user-defined year boundaries, which may introduce mismatches between subsequent
573 years to be propagated through the age model, even in ideal datasets such as **Case 1** (Fig. 5B8B; see
574 also **Supplementary Methods**). By comparison, the overall accuracy of ShellChron is much more stable
575 within and between datasets of different length, while rarely introducing offsets of more than a month.
576 More importantly, where ShellChron takes into account the uncertainty on input parameters, this
577 uncertainty is not considered in most previous models (the MoGroFun model of Goodwin et al., 2003
578 being the exception). The added uncertainty caused by input error is higher in less regular (sinusoidal)
579 $\delta^{18}\text{O}_c$ records and in records with lower sampling resolution, causing the uncertainties on the Judd et
580 al., model reported here for the ideal, high-resolution **Case 1** dataset to be over-optimistic. If
581 ShellChron's model accuracy is insufficient, its modular character allows the user to run the SCEUA
582 algorithm to within more precise optimization criteria by changing the model parameters (see [S13section](#)
583 [4.1](#)). However, this adaptation comes at a cost of longer computation times.

584 The estimated uncertainty envelope (95% confidence interval) on the modelled age calculated by the
585 error propagation algorithm in ShellChron ($24.4.7 \pm 14.6.5$ d) on average slightly underestimates the
586 actual offset between modelled age and real age in the **Case 1** record ($31.9.3 \pm 24.13.1$ d; $\text{difference} \leftarrow$
587 0.05 ; Fig. 5C8C). The foremost difference between modelled and real uncertainty on the result is that
588 the modelled uncertainty yields a more smoothed record of uncertainty compared to the record of actual
589 offset of the model (Fig. 5C8C). ShellChron's uncertainty calculations are partly based on comparing
590 overlapping model windows, thereby smoothing out short term variations in model offset. The
591 uncertainty of the model result (both real and modelled) shows regular variability with a period of half a
592 year (Fig. 5C8C). Comparing this variability with the phase of the record (of which 6 years are plotted
593 in Fig. 3A6A) reveals that the uncertainty of the model is positively correlated to the slope of the $\delta^{18}\text{O}_c$
594 record. This is expected, because in parts of the record with steep $\delta^{18}\text{O}_c$ -[depth-distance](#) slopes, the local
595 age model result is more sensitive to small changes in the [depth-sampling-distance](#) domain, caused
596 either by uncertainty in the model fit or propagated uncertainty on the [depth-valuesampling distance](#)
597 defined by the user. The slight seasonal variability in model accuracy in Case 1 is also shown in Fig.
598 6C and comprises a difference in uncertainty of up to 10 days depending on the time of year in which
599 the datapoint is found.

600

601

602 5. Applications and discussion

603 Its new features compared to previous age model routines make ShellChron a versatile package for
604 creating age models in a range of high-resolution paleoclimate records. The discussion above
605 demonstrates that ShellChron can reconstruct the age of individual $\delta^{18}\text{O}_c$ samples within monthly
606 precision. This level of precision is sufficient for accurate reconstructions of seasonality, defined as the
607 difference between warmest and coldest month (following USGS definitions; O'Donnell and Ignizio,
608 2012). While an improvement on this uncertainty could be of potential interest for ultra-high-resolution
609 paleoclimate studies (e.g. sub-daily variability, see Sano et al., 2012; Yan et al., 2020; de Winter et al.,
610 2020a), the increase in computation time and the sampling resolution such detailed age models demand
611 render age modelling from $\delta^{18}\text{O}_c$ records inefficient for this purpose (see sections 4.1 and 4.4). The
612 sampling resolution for high-resolution carbonate $\delta^{18}\text{O}_c$ records in the literature does not typically exceed
613 ~~0.1 mm~~ 100 μm due to limitations in sampling acquisition (e.g. micromilling), which even in fast-growing
614 archives limits the resolution of these records to several days at best (see Gagan et al., 1994; Van
615 Rampelbergh et al., 2014; de Winter et al., 2020c). While in some archives, high-resolution (< 100 μm)
616 trace element records could be used to capture variability beyond this limit, the monthly age resolution
617 of ShellChron is sufficient for most typical high-resolution paleoclimate studies.

618 The ability to produce uninterrupted age models from multi-year records while considering both
619 variability in $\delta^{18}\text{O}_w$ and uncertainties on input parameters represent major advantages of ShellChron
620 over previous age modelling solutions. As a result, ShellChron can be applied on a wide range of
621 carbonate archives (see Fig. 4-7 and Table 2). However, testing ShellChron on different records
622 highlights the limitations of the model inherited through its underlying assumptions. The most accurate
623 model results are obtained on records with minimal growth rate and $\delta^{18}\text{O}_w$ variability and a nearly
624 sinusoidal $\delta^{18}\text{O}_c$ record, such as tropical coral records (Fig. 4A7A; Gagan et al., 1994). In records where
625 large seasonal variability in growth rate and $\delta^{18}\text{O}_w$ does occur, such as in intertidal oyster shells,
626 ShellChron's accuracy slightly decreases, especially near growth hiatuses in the record (see Fig. 4B7B;
627 Ullmann et al., 2010). A worst-case scenario is represented by the speleothem record, which not only
628 suffers from much slower and more unpredictable growth rates and contains a comparatively small
629 annual range in $\delta^{18}\text{O}_c$, but it responds to $\delta^{18}\text{O}_w$ variability in drip water in the cave rather than temperature

630 seasonality, one of the assumptions underlying the current version of ShellChron (**Fig. 4C7C**;
631 Vansteenberghe et al., 2019). Despite these problems, ShellChron yields an age model that is
632 remarkably accurate on an annual timescale, which is as good as, or better than, the best age model
633 that can be obtained by applying layer counting on the most clearly laminated parts of the speleothem
634 (e.g. Verheyden et al., 2006). It must be noted that, while ~~this is an encouraging result~~ the close fit
635 between modelled $\delta^{18}\text{O}_c$ and speleothem $\delta^{18}\text{O}_c$ data ($\rho = 0.92$; $\sigma = 0.08\%$) is encouraging, a major
636 reason for the model's success is the fact that the Proserpine speleothem used in this example is known
637 to receive significantly seasonal (though not sinusoidal) drip water volumes and concentrations (Van
638 Rampelbergh et al., 2014). Variability in drip water properties and cave temperatures are known to differ
639 strongly between cave systems, ~~and ShellChron can therefore only be applied with confidence on~~
640 ~~speleothem records if consistent seasonal variability in these parameters can be demonstrated~~
641 (Fairchild et al., 2006; Lachniet, 2009). For ShellChron (or any other $\delta^{18}\text{O}_c$ -based age model) to work
642 reliably in speleothem records, consistent seasonal variability in either temperature or $\delta^{18}\text{O}_w$ should be
643 demonstrated to significantly influence the $\delta^{18}\text{O}_c$ variability in the record. In practice, these constraints
644 make ShellChron applicable in speleothems for which the cave environment varies in response to the
645 seasonal cycle, such as localities overlain by thin epikarst, well-ventilated caves or speleothems situated
646 close to the cave entrance (Verheyden et al., 2006; Feng et al., 2013; Baker et al., 2021)

647 The difficulty of applying age model routines on speleothem records highlights one of the main
648 advantages of ShellChron over pre-existing age model routines, namely its modular character. Since
649 $\delta^{18}\text{O}_c$ records from some carbonate archives, such as speleothems, cannot be described by the
650 standard combination of temperature and growth rate sinusoids on which ShellChron is based (in its
651 current version), the possibility to adapt the “building block” functions used to approximate these $\delta^{18}\text{O}_c$
652 records (*d18O_model*, *temperature_curve* and *growth_rate_curve*; see **Fig. 1**) while leaving the core
653 structure of ShellChron intact greatly augments the versatility of the model. The freedom to adapt the
654 building blocks used to approximate the $\delta^{18}\text{O}_c$ record theoretically enables ShellChron to model sub-
655 annual age-~~depth-distance~~ relationships in any record as long as the seasonal variability in the variables
656 used to model the input data are predictable and can be represented by a function. For example, since
657 speleothem $\delta^{18}\text{O}_c$ records often depend on variability in the $\delta^{18}\text{O}_w$ value of the drip water, a function
658 describing this variability through the year can replace the *temperature_curve* function to create more
659 accurate sub-annual age models for speleothems (e.g. Matthey et al., 2008; Lachniet, 2009; Van

Formatted: Subscript

660 Rampelbergh et al., 2014). Similarly, the *growth_rate_curve* function can be modified in case the default
661 skewed sinusoid does not accurately describe the extension rate of the record under study, and the
662 *d18O_model* function can be adapted to feature the most fitting $\delta^{18}\text{O}_c$ -temperature or $\delta^{18}\text{O}_c$ - $\delta^{18}\text{O}_w$
663 relationship. Note that the flexibility of this approach is limited by the expression of the annual cycle in
664 the $\delta^{18}\text{O}_c$ record. The $\delta^{18}\text{O}_c$ -based dating approach in ShellChron will therefore have severe trouble
665 dating records in which the annual $\delta^{18}\text{O}_c$ variability is severely dampened, such as speleothems in
666 deeper cave systems (e.g. Vansteenberghe et al., 2016), or in which annual $\delta^{18}\text{O}_c$ variability is not
667 sinusoidal, such as tropical records with bimodal temperature or precipitation seasonality (Knoben et
668 al., 2018).

669 ~~By extension,~~ flexibility in the definition of “building block” functions used to approximate the input data
670 paves the way for future application beyond carbonate $\delta^{18}\text{O}_c$ records. The seasonal variability in $\delta^{18}\text{O}$ in
671 some ice cores can be approximated by a stable and unbiased temperature relationship (van Ommen
672 and Morgan, 1997). ShellChron can therefore be modified to date sub-annual samples in these ice core
673 records and reconstruct seasonal variability in the high latitudes through the Quaternary. Similarly, inter-
674 annual $\delta^{18}\text{O}$ variability in tree ring records are demonstrated to record variability in precipitation through
675 the year, and this variability can be modelled to improve sub-annual age models in these records (Xu et
676 al., 2016). More generally, the field of dendrochemistry has recently developed additional chemical
677 proxies for seasonality (e.g. trace element concentrations), which can be measured on smaller sample
678 volumes (and thus greater resolution) to obtain ultra-high-resolution records on which (sub-annual)
679 dating can be based (e.g. Poussart et al., 2006; Superville et al., 2017). A similar development has taken
680 place in the study of carbonate bio-archives such as corals and mollusks, of which some show strong,
681 predictable seasonal variability in trace elements (e.g. Mg/Ca and Sr/Ca ratios) which can be used to
682 accurately date these records (de Villiers et al., 1995; Sosdian et al., 2006; Durham et al., 2017). Minor
683 changes in the “building block” functions using empirical transfer functions for these trace element
684 records will enable ShellChron to capitalize on these relationships and reconstruct sub-annual growth
685 rates with improved precision due to the higher precision with which these proxies can be measured
686 compared to $\delta^{18}\text{O}_c$ records. Finally, the application of ShellChron for age model construction is not
687 necessarily limited to the seasonal cycle, as other major cycles in climate (e.g. tidal, diurnal or
688 Milankovitch cycles) leave similar marks on climate records and can thus be used as basis for age
689 modelling (e.g. Sano et al., 2012; Huyghe et al., 2019; de Winter et al., 2020a; Sinnesael et al., 2020).

690 It must be noted that, since ShellChron was developed for modeling based on annual periodicity,
691 applying it on other timescales would require more thorough adaptation of the model code than merely
692 adapting the “building block” functions to support additional proxy systems.

693 While age reconstructions are the main aim of ShellChron, the model also yields information about the
694 temperature and growth rate parameters used in each simulation window to approximate the local $\delta^{18}\text{O}_c$
695 curve (see parameter matrix in Fig. 1 and SI6). These parameters hold key information about the
696 response of the archive to seasonal changes in the environment, such as the season of growth,
697 relationships between growth rate and temperature and the temperature range that is recorded. By
698 eCombining these parameters with records of influential environmental variables such as seawater
699 chlorophyll concentration or local precipitation patterns, ~~much can be learned about the yields~~
700 information about the response of the climate archive ~~itself and its response~~ to environmental variables,
701 in addition to the climate or environmental change it records. Study examples include the relationship
702 between growth rate of marine calcifiers and phytoplankton abundance or the correlation between
703 precipitation patterns and chemical variability in speleothems. While such discussion is beyond the
704 scope of this work, examples of parameter distributions are provided in SI5, and the application of
705 modelled growth rate parameters in bivalve sclerochronology is discussed in more detail in Judd et al.
706 (2018). Note that the sliding window approach of ShellChron produces records of changing temperature
707 and growth rate parameters at the scale of individual samples (albeit smoothed by the sliding window
708 approach) rather than annually, as in Judd et al. (2018).

709

710 6. Conclusions

711 ShellChron offers a novel, open-source solution to the problem of dating carbonate archives for high-
712 resolution paleoclimate reconstruction on a sub-annual scale. Based on critical evaluation of previous
713 age models, building on their strengths while attempting to eliminate their weaknesses, ShellChron
714 provides continuous age models based on $\delta^{18}\text{O}_c$ -profiles in these archives with monthly accuracy, taking
715 into account considering the uncertainties associated with both the model itself and the input data. The
716 monthly accuracy of the model, as tested on a range of virtual and natural datasets, enables its
717 application for age determination in studies of seasonal climate and environmental variability. Higher
718 accuracies can be reached at the cost of longer computation times by adapting the model parameters,

719 but age determinations far beyond the monthly scale are unlikely to be feasible considering the
720 limitations on sampling resolution and measurement uncertainties on $\delta^{18}\text{O}_c$ records. ShellChron's
721 computation times on datasets with sampling resolutions typical for the paleoclimatology field (up to 20
722 samples/yr) remain practical and ~~competitive with~~comparable to previous model solutions, despite
723 adding several features that improve the versatility and interpretation of model results. Its modular
724 design allows ShellChron to be adapted to different situations with comparative ease. It thereby
725 functions as a platform for age-~~depth~~distance modelling on a wide range of climate and environmental
726 archives and is not limited in its application to the $\delta^{18}\text{O}_c$ proxy, the carbonate substrate or even to the
727 annual cycle, as long as the relationship between the proxy and the extension rate of the archive on a
728 given time scale can be parameterized. Future improvements will capitalize on this variability, expanding
729 ShellChron beyond its current dependency on the $\delta^{18}\text{O}_c$ -temperature relationship in carbonates.
730 Members of the high-resolution paleoclimate community are invited to contribute to this effort by
731 adapting the model for their purpose.

732

733 **Code availability**

734 ShellChron is worked out into a fully functioning package for the open-source computational language
735 R (version 3.5.0 or later; R Core Team, 2020). The most recent full version (v0.~~2.84.0~~2.9.9000) of the ShellChron
736 passed the code review of the Comprehensive R Archive Network (CRAN) and is freely available for
737 download as an R package on the CRAN server (see <https://CRAN.R-project.org/package=ShellChron>).
738 The CRAN server entry also includes detailed line-by-line documentation of the code and working
739 examples for every function. In addition, the latest development version of ShellChron (~~currently~~
740 ~~v0.2.9.9000~~) is available on GitHub (<https://github.com/nielsidewinter/ShellChron>). Those interested in
741 adapting ShellChron for their research purposes are invited to do so here. Code and documentation,
742 together with all supplementary files belonging to this study, are also available on the open-source online
743 repository Zenodo (<http://doi.org/10.5281/zenodo.4288344>).

744

745 **Author contribution**

746 NJW designed the study, wrote the model script, carried out the test calculations and wrote the
747 manuscript.

748

749 **Competing interests**

750 There were no competing interests to declare.

751

752 **Acknowledgements**

753 This research project is part of the UNBIAS project funded by the European Commission through a
754 Marie Curie Individual Fellowship (MSCA-IF; grant number: 843011) and the Flemish Research Council
755 (FWO; junior postdoc grant, project number: 12ZB220N). Thanks go to Emily Judd for discussions about
756 the workings of the Judd et al. (2018) model and its potential adaptation beyond aragonitic mollusk
757 shells. High-resolution temperature and salinity data from the NIOZ jetty which underlie the **Texel**
758 dataset and the noise added to the idealized **Case 1** dataset were kindly provided by Eric Wagemakers
759 and Sonja van Leeuwen (Royal Dutch Institute for Sea Research, the Netherlands). The $\delta^{18}\text{O}_c$ data
760 series from the *Crassostrea gigas* (**oyster**) and Proserpine stalagmite (**speleothem**) were generously
761 provided by dr. Clemens V. Ullmann (University of Exeter, UK) and dr. Stef Vansteenberge (Vrije
762 Universiteit Brussel, Belgium), respectively. Raw data from the *Porites lutea* coral dataset were obtained
763 with help of the WebPlotDigitizer (<https://automeris.io/WebPlotDigitizer/>) developed by Ankit Rohatgi.
764 Preparation of the ShellChron model into an R package would not have been possible without the helpful
765 instructions by Fong Chun Chan ([https://tinyheero.github.io/jekyll/update/2015/07/26/making-your-first-](https://tinyheero.github.io/jekyll/update/2015/07/26/making-your-first-R-package.html)
766 [R-package.html](https://tinyheero.github.io/jekyll/update/2015/07/26/making-your-first-R-package.html)), Hilary Parker ([https://hilaryparker.com/2014/04/29/writing-an-r-package-from-](https://hilaryparker.com/2014/04/29/writing-an-r-package-from-scratch/)
767 [scratch/](https://hilaryparker.com/2014/04/29/writing-an-r-package-from-scratch/)) and Hadley Wickham (<https://r-pkgs.org/release.html>) as well as the insightful and inspiring
768 discussions on R coding and statistics with Ilja Kocken (Utrecht University). In addition, distribution of
769 the code in an organized way was made possible thanks to Git (<https://git-scm.com/>) and Github
770 (<https://github.com/>) and the R Project Team (<https://www.r-project.org/>), with special thanks to Uwe
771 Ligges (University of Dortmund, Germany) and Gregor Seyer (University of Vienna, Austria) for their
772 comments on initial submissions of the package to the CRAN database. Thanks go to William A. Huber
773 (<https://www.analysisandinference.com/team/william-a-huber-phd>) for providing a practical general

774 solution to the peak identification problem in the *cumulative_day* function (see *peakid* function and
775 https://rpubs.com/mengxu/peak_detection).
776

777 **References**

- 778 [Bainai D., Guo W., Spötl C., Coplen T. B., Methner K., Löffler N., Krsnik E., Gischler E., Hansen M.,](#)
779 [Henkel D., Price G. D., Raddatz J., Scholz D. and Fiebig J. \(2020\) Dual clumped isotope thermometry](#)
780 [resolves kinetic biases in carbonate formation temperatures. *Nature Communications* **11**, 4005.](#)
- 781 [Baker A., Mariethoz G., Comas-Bru L., Hartmann A., Frisia S., Borsato A., Treble P. C. and Asrat A.](#)
782 [\(2021\) The Properties of Annually Laminated Stalagmites-A Global Synthesis. *Reviews of Geophysics*](#)
783 [59, e2020RG000722.](#)
- 784 [Baldini J. U. L., McDermott F., Hoffmann D. L., Richards D. A. and Clipson N. \(2008\) Very high-](#)
785 [frequency and seasonal cave atmosphere PCO₂ variability: Implications for stalagmite growth and](#)
786 [oxygen isotope-based paleoclimate records. *Earth and Planetary Science Letters* **272**, 118–129.](#)
- 787 [Brand W. A., Coplen T. B., Vogl J., Rosner M. and Prohaska T. \(2014\) Assessment of international](#)
788 [reference materials for isotope-ratio analysis \(IUPAC Technical Report\). *Pure and Applied Chemistry*](#)
789 [86, 425–467.](#)
- 790 [de Brauwere A., De Ridder F., Pintelon R., Schoukens J. and Dehairs F. \(2009\) A comparative study](#)
791 [of methods to reconstruct a periodic time series from an environmental proxy record. *Earth-Science*](#)
792 [Reviews](#) **95**, 97–118.
- 793 [Butler P. G., Wanamaker A. D., Scourse J. D., Richardson C. A. and Reynolds D. J. \(2013\) Variability](#)
794 [of marine climate on the North Icelandic Shelf in a 1357-year proxy archive based on growth](#)
795 [increments in the bivalve *Arctica islandica*. *Palaeogeography, Palaeoclimatology, Palaeoecology* **373**,](#)
796 [141–151.](#)
- 797 [Chauvaud L., Lorrain A., Dunbar R. B., Paulet Y.-M., Thouzeau G., Jean F., Guarini J.-M. and](#)
798 [Mucciarone D. \(2005\) Shell of the Great Scallop *Pecten maximus* as a high-frequency archive of](#)
799 [paleoenvironmental changes. *Geochemistry, Geophysics, Geosystems* **6**.](#)
- 800 [Coplen T. B. \(2007\) Calibration of the calcite–water oxygen-isotope geothermometer at Devils Hole,](#)
801 [Nevada, a natural laboratory. *Geochimica et Cosmochimica Acta* **71**, 3948–3957.](#)
- 802 [Daëron M., Drysdale R. N., Peral M., Huyghe D., Blamart D., Coplen T. B., Lartaud F. and Zanchetta](#)
803 [G. \(2019\) Most Earth-surface calcites precipitate out of isotopic equilibrium. *Nature Communications*](#)
804 [10, 429.](#)
- 805 [Daëron M., Guo W., Eiler J., Genty D., Blamart D., Boch R., Drysdale R., Maire R., Wainer K. and](#)
806 [Zanchetta G. \(2011\) ¹³C/¹⁸O clumping in speleothems: Observations from natural caves and](#)
807 [precipitation experiments. *Geochimica et Cosmochimica Acta* **75**, 3303–3317.](#)
- 808 [De Ridder F., de Brauwere A., Pintelon R., Schoukens J., Dehairs F., Baeyens W. and Wilkinson B. H.](#)
809 [\(2007\) Comment on: Paleoclimatic inference from stable isotope profiles of accretionary biogenic](#)
810 [hardparts—a quantitative approach to the evaluation of incomplete data, by Wilkinson, BH, Ivany, LC,](#)
811 [2002. *Palaeogeogr. Palaeocl. Palaeoecol.* **185**, 95–114. *Palaeogeography, Palaeoclimatology,*](#)
812 [*Palaeoecology* **248**, 473–476.](#)
- 813 [DeCarlo T. M. and Cohen A. L. \(2017\) Dissepiments, density bands and signatures of thermal stress](#)
814 [in *Porites* skeletons. *Coral Reefs* **36**, 749–761.](#)
- 815 [Dettman D. L., Reische A. K. and Lohmann K. C. \(1999\) Controls on the stable isotope composition of](#)
816 [seasonal growth bands in aragonitic fresh-water bivalves \(Unionidae\). *Geochimica et Cosmochimica*](#)
817 [Acta](#) **63**, 1049–1057.
- 818 [Duan Q., Sorooshian S. and Gupta V. \(1992\) Effective and efficient global optimization for conceptual](#)
819 [rainfall-runoff models. *Water resources research* **28**, 1015–1031.](#)
- 820 [Dunbar R. B. and Wellington G. M. \(1981\) Stable isotopes in a branching coral monitor seasonal](#)
821 [temperature variation. *Nature* **293**, 453–455.](#)
- 822 [Durham S. R., Gillikin D. P., Goodwin D. H. and Dietl G. P. \(2017\) Rapid determination of oyster](#)
823 [lifespans and growth rates using LA-ICP-MS line scans of shell Mg/Ca ratios. *Palaeogeography,*](#)
824 [*Palaeoclimatology, Palaeoecology*.](#)

Formatted: Font: (Default) Arial, 10 pt

Formatted: Indent: First line: 0"

825 [Epstein S., Buchsbaum R., Lowenstam H. A. and Urey H. C. \(1953\) Revised carbonate-water isotopic](#)
826 [temperature scale. *Geological Society of America Bulletin* **64**, 1315–1326.](#)

827 [Evans M. N. and Schrag D. P. \(2004\) A stable isotope-based approach to tropical dendroclimatology1](#)
828 [1Associate editor: D. W. Lea. *Geochimica et Cosmochimica Acta* **68**, 3295–3305.](#)

829 [Fairchild I. J., Smith C. L., Baker A., Fuller L., Spötl C., Matthey D., McDermott F., and others \(2006\)](#)
830 [Modification and preservation of environmental signals in speleothems. *Earth-Science Reviews* **75**,](#)
831 [105–153.](#)

832 [Feng W., Casteel R. C., Banner J. L. and Heinze-Fry A. \(2014\) Oxygen isotope variations in rainfall,](#)
833 [drip-water and speleothem calcite from a well-ventilated cave in Texas, USA: Assessing a new](#)
834 [speleothem temperature proxy. *Geochimica et Cosmochimica Acta* **127**, 233–250.](#)

835 [Frisia S., Borsato A., Fairchild I. J. and McDermott F. \(2000\) Calcite fabrics, growth mechanisms, and](#)
836 [environments of formation in speleothems from the Italian Alps and southwestern Ireland. *Journal of*](#)
837 [Sedimentary Research](#) **70**, 1183–1196.

838 [Gagan M. K., Chivas A. R. and Isdale P. J. \(1994\) High-resolution isotopic records from corals using](#)
839 [ocean temperature and mass-spawning chronometers. *Earth and Planetary Science Letters* **121**, 549–](#)
840 [558.](#)

841 [Goodwin D. H., Paul P. and Wissink C. L. \(2009\) MoGroFunGen: A numerical model for reconstructing](#)
842 [intra-annual growth rates of bivalve molluscs. *Palaeogeography, Palaeoclimatology, Palaeoecology*](#)
843 [276, 47–55.](#)

844 [Goodwin D. H., Schöne B. R. and Dettman D. L. \(2003\) Resolution and Fidelity of Oxygen Isotopes as](#)
845 [Paleotemperature Proxies in Bivalve Mollusk Shells: Models and Observations. *PALAIOS* **18**, 110–](#)
846 [125.](#)

847 [Grossman E. L. and Ku T.-L. \(1986\) Oxygen and carbon isotope fractionation in biogenic aragonite:](#)
848 [temperature effects. *Chemical Geology: Isotope Geoscience section* **59**, 59–74.](#)

849 [Huybers P. and Curry W. \(2006\) Links between annual, Milankovitch and continuum temperature](#)
850 [variability. *Nature* **441**, 329.](#)

851 [Huyghe D., de Rafelis M., Ropert M., Mouchi V., Emmanuel L., Renard M. and Lartaud F. \(2019\) New](#)
852 [insights into oyster high-resolution hinge growth patterns. *Mar Biol* **166**, 48.](#)

853 [IPCC \(2018\) GLOBAL WARMING OF 1.5 °C an IPCC special report on the impacts of global warming](#)
854 [of 1.5 °C above pre-industrial levels and related global greenhouse gas emission pathways, in the](#)
855 [context of strengthening the global response to the threat of climate change, sustainable development,](#)
856 [and efforts to eradicate poverty.](#)

857 [Ivany L. C. and Runnegar B. \(2010\) Early Permian seasonality from bivalve \$\delta^{18}\text{O}\$ and implications for](#)
858 [the oxygen isotopic composition of seawater. *Geology* **38**, 1027–1030.](#)

859 [Jones D. S. \(1983\) Sclerochronology: Reading the Record of the Molluscan Shell: Annual growth](#)
860 [increments in the shells of bivalve molluscs record marine climatic changes and reveal surprising](#)
861 [longevity. *American Scientist* **71**, 384–391.](#)

862 [Jones D. S. and Quitmyer I. R. \(1996\) Marking Time with Bivalve Shells: Oxygen Isotopes and Season](#)
863 [of Annual Increment Formation. *PALAIOS* **11**, 340–346.](#)

864 [Judd E. J., Wilkinson B. H. and Ivany L. C. \(2018\) The life and time of clams: Derivation of intra-annual](#)
865 [growth rates from high-resolution oxygen isotope profiles. *Palaeogeography, Palaeoclimatology,*](#)
866 [Palaeoecology](#) **490**, 70–83.

867 [Kim S.-T. and O'Neil J. R. \(1997\) Equilibrium and nonequilibrium oxygen isotope effects in synthetic](#)
868 [carbonates. *Geochimica et Cosmochimica Acta* **61**, 3461–3475.](#)

869 [Knoben W. J. M., Woods R. A. and Freer J. E. \(2019\) Global bimodal precipitation seasonality: A](#)
870 [systematic overview. *International Journal of Climatology* **39**, 558–567.](#)

871 [Lachniet M. S. \(2009\) Climatic and environmental controls on speleothem oxygen-isotope values.](#)
872 [Quaternary Science Reviews](#) **28**, 412–432.

873 [Le Tissier M. D. A., Clayton B., Brown B. E. and Davis P. S. \(1994\) Skeletal correlates of coral density](#)
874 [banding and an evaluation of radiography as used in sclerochronology. *Marine Ecology Progress*](#)
875 [Series **110**, 29–44.](#)

876 [LeGrande A. N. and Schmidt G. A. \(2006\) Global gridded data set of the oxygen isotopic composition](#)
877 [in seawater. *Geophysical research letters* **33**.](#)

878 [Lough J. M. \(2010\) Climate records from corals. *WIREs Climate Change* **1**, 318–331.](#)

879 [Mahé K., Bellamy E., Lartaud F. and Raféls M. de \(2010\) Calcein and manganese experiments for](#)
880 [marking the shell of the common cockle \(*Cerastoderma edule*\): tidal rhythm validation of increments](#)
881 [formation. *Aquat. Living Resour.* **23**, 239–245.](#)

882 [Mattey D., Lowry D., Duffet J., Fisher R., Hodge E. and Frisia S. \(2008\) A 53 year seasonally resolved](#)
883 [oxygen and carbon isotope record from a modern Gibraltar speleothem: Reconstructed drip water and](#)
884 [relationship to local precipitation. *Earth and Planetary Science Letters* **269**, 80–95.](#)

885 [McCrea J. M. \(1950\) On the Isotopic Chemistry of Carbonates and a Paleotemperature Scale. *J.*
886 \[Chem. Phys.\]\(#\) **18**, 849–857.](#)

887 [Mitchell Jr. J. M. \(1976\) An overview of climatic variability and its causal mechanisms. *Quaternary*
888 \[Research\]\(#\) **6**, 481–493.](#)

889 [Mohr R. C., Tobin T. S., Petersen S. V., Dutton A. and Oliphant E. \(2020\) Subannual stable isotope](#)
890 [records reveal climate warming and seasonal anoxia associated with two extinction intervals across](#)
891 [the Cretaceous-Paleogene boundary on Seymour Island, Antarctica. *Geology* **48**, 1131–1136.](#)

892 [Müller P., Taylor M. H., Klicpera A., Wu H. C., Michel J. and Westphal H. \(2015\) Food for thought:](#)
893 [Mathematical approaches for the conversion of high-resolution sclerochronological oxygen isotope](#)
894 [records into sub-annually resolved time series. *Palaeogeography, Palaeoclimatology, Palaeoecology*](#)
895 [440, 763–776.](#)

896 [O'Donnell M. S. and Ignizio D. A. \(2012\) Bioclimatic predictors for supporting ecological applications in](#)
897 [the conterminous United States. *US Geological Survey Data Series* **691**.](#)

898 [Ommen T. D. van and Morgan V. \(1997\) Calibrating the ice core paleothermometer using seasonality.](#)
899 [Journal of Geophysical Research: Atmospheres](#) **102**, 9351–9357.

900 [Poussart P. M., Myneni S. C. B. and Lanzirotti A. \(2006\) Tropical dendrochemistry: A novel approach](#)
901 [to estimate age and growth from ringless trees. *Geophysical Research Letters* **33**.](#)

902 [R Core Team \(2020\) *R: A Language and Environment for Statistical Computing*.](#), R Foundation for
903 [Statistical Computing, Vienna, Austria.](#)

904 [Rohling E. J. \(2013\) Oxygen isotope composition of seawater. *The Encyclopedia of Quaternary*
905 \[Science. Amsterdam: Elsevier\]\(#\) **2**, 915–922.](#)

906 [Saenger C., Gabitov R. I., Farmer J., Watkins J. M. and Stone R. \(2017\) Linear correlations in bamboo](#)
907 [coral \$\delta^{13}\text{C}\$ and \$\delta^{18}\text{O}\$ sampled by SIMS and micromill: Evaluating paleoceanographic potential and](#)
908 [biomineralization mechanisms using \$\delta^{11}\text{B}\$ and \$\Delta 47\$ composition. *Chemical Geology* **454**, 1–14.](#)

909 [Sano Y., Kobayashi S., Shirai K., Takahata N., Matsumoto K., Watanabe T., Sowa K. and Iwai K.](#)
910 [\(2012\) Past daily light cycle recorded in the strontium/calcium ratios of giant clam shells. *Nature*](#)
911 [Communications](#) **3**, 761.

912 [Schöne B. R., Fiebig J., Pfeiffer M., Gleß R., Hickson J., Johnson A. L., Dreyer W. and Oschmann W.](#)
913 [\(2005\) Climate records from a bivalved Methuselah \(*Arctica islandica*, Mollusca: Iceland\).](#)
914 [Palaeogeography, Palaeoclimatology, Palaeoecology](#) **228**, 130–148.

915 [Schöne B. R. and Gillikin D. P. \(2013\) Unraveling environmental histories from skeletal diaries —](#)
916 [Advances in sclerochronology. *Palaeogeography, Palaeoclimatology, Palaeoecology* **373**, 1–5.](#)

917 [Schöne B. R., Zhang Z., Radermacher P., Thébault J., Jacob D. E., Nunn E. V. and Maurer A.-F.](#)
918 [\(2011\) Sr/Ca and Mg/Ca ratios of ontogenetically old, long-lived bivalve shells \(*Arctica islandica*\) and](#)
919 [their function as paleotemperature proxies. *Palaeogeography, Palaeoclimatology, Palaeoecology* **302**,](#)
920 [52–64.](#)

921 [Sinnesael M., De Vleeschouwer D., Zeeden C., Batenburg S. J., Da Silva A.-C., de Winter N. J.,](#)
922 [Dinarès-Turell J., Drury A. J., Gambacorta G. and Hilgen F. J. \(2019\) The Cyclostratigraphy](#)
923 [Intercomparison Project \(CIP\): consistency, merits and pitfalls. *Earth-Science Reviews*, 102965.](#)

924 [Sosdian S., Gentry D. K., Lear C. H., Grossman E. L., Hicks D. and Rosenthal Y. \(2006\) Strontium to](#)
925 [calcium ratios in the marine gastropod *Conus ermineus*: Growth rate effects and temperature](#)
926 [calibration. *Geochemistry, Geophysics, Geosystems* 7.](#)

927 [Steuber T., Rauch M., Masse J.-P., Graaf J. and Malkoč M. \(2005\) Low-latitude seasonality of](#)
928 [Cretaceous temperatures in warm and cold episodes. *Nature* 437, 1341–1344.](#)

929 [Superville P.-J., De Winter N., Phung A. T., Proix N., Baeyens W. and Gao Y. \(2017\) Radial metal](#)
930 [concentration profiles in trees growing on highly contaminated soils. *Chemosphere* 172, 80–88.](#)

931 [Tarutani T., Clayton R. N. and Mayeda T. K. \(1969\) The effect of polymorphism and magnesium](#)
932 [substitution on oxygen isotope fractionation between calcium carbonate and water. *Geochimica et*](#)
933 [Cosmochimica Acta 33, 987–996.](#)

934 [Treble P. C., Schmitt A. K., Edwards R. L., McKeegan K. D., Harrison T. M., Grove M., Cheng H. and](#)
935 [Wang Y. J. \(2007\) High resolution Secondary Ionisation Mass Spectrometry \(SIMS\) \$\delta^{18}\text{O}\$ analyses of](#)
936 [Hulu Cave speleothem at the time of Heinrich Event 1. *Chemical Geology* 238, 197–212.](#)

937 [Ullmann C. V., Böhm F., Rickaby R. E., Wiechert U. and Korte C. \(2013\) The Giant Pacific Oyster](#)
938 [\(*Crassostrea gigas*\) as a modern analog for fossil ostreoids: isotopic \(Ca, O, C\) and elemental \(Mg/Ca,](#)
939 [Sr/Ca, Mn/Ca\) proxies. *Geochemistry, Geophysics, Geosystems* 14, 4109–4120.](#)

940 [Ullmann C. V. and Korte C. \(2015\) Diagenetic alteration in low-Mg calcite from macrofossils: a review.](#)
941 [Geological Quarterly 59, 3–20.](#)

942 [Ullmann C. V., Wiechert U. and Korte C. \(2010\) Oxygen isotope fluctuations in a modern North Sea](#)
943 [oyster \(*Crassostrea gigas*\) compared with annual variations in seawater temperature: Implications for](#)
944 [palaeoclimate studies. *Chemical Geology* 277, 160–166.](#)

945 [Urban F. E., Cole J. E. and Overpeck J. T. \(2000\) Influence of mean climate change on climate](#)
946 [variability from a 155-year tropical Pacific coral record. *Nature* 407, 989–993.](#)

947 [Urey H. C. \(1948\) Oxygen Isotopes in Nature and in the Laboratory. *Science* 108, 489–496.](#)

948 [Van Rampelbergh M., Verheyden S., Allan M., Quinif Y., Keppens E. and Claeys P. \(2014\) Seasonal](#)
949 [variations recorded in cave monitoring results and a 10 year monthly resolved speleothem \$\delta^{18}\text{O}\$ and](#)
950 [\$\delta^{13}\text{C}\$ record from the Han-sur-Lesse cave, Belgium. *Climate of the Past Discussions* 10, 1821–1856.](#)

951 [Vansteenberghe S., Verheyden S., Cheng H., Edwards R. L., Keppens E. and Claeys P. \(2016\)](#)
952 [Paleoclimate in continental northwestern Europe during the Eemian and early Weichselian \(125–](#)
953 [97 ka\): insights from a Belgian speleothem. *Clim. Past* 12, 1445–1458.](#)

954 [Vansteenberghe S., Winter N. de, Sinnesael M., Verheyden S., Goderis S., Malderen S. J. M. V.,](#)
955 [Vanhaecke F. and Claeys P. \(2019\) Reconstructing seasonality through stable isotope and trace](#)
956 [element analysis of the Proserpine stalagmite, Han-sur-Lesse Cave, Belgium: indications for climate-](#)
957 [driven changes during the last 400 years. *Climate of the Past Discussions*, 1–32.](#)

958 [Verheyden S., Baele J.-M., Keppens E., Genty D., Cattani O., Cheng H., LAWRENCE E., ZHANG H.,](#)
959 [Van Strijdonck M. and Quinif Y. \(2006\) The Proserpine stalagmite \(Han-Sur-Lesse Cave, Belgium\):](#)
960 [preliminary environmental interpretation of the last 1000 years as recorded in a layered speleothem.](#)
961 [Geologica Belgica.](#)

962 [de Villiers S., Nelson B. K. and Chivas A. R. \(1995\) Biological controls on coral Sr/Ca and \$\delta^{18}\text{O}\$](#)
963 [reconstructions of sea surface temperatures. *Science* 269, 1247.](#)

964 [Wang Y. J., Cheng H., Edwards R. L., An Z. S., Wu J. Y., Shen C.-C. and Dorale J. A. \(2001\) A High-](#)
965 [Resolution Absolute-Dated Late Pleistocene Monsoon Record from Hulu Cave, China. *Science* 294,](#)
966 [2345–2348.](#)

967 [Watkins J. M., Hunt J. D., Ryerson F. J. and DePaolo D. J. \(2014\) The influence of temperature, pH,](#)
968 [and growth rate on the \$\delta^{18}\text{O}\$ composition of inorganically precipitated calcite. *Earth and Planetary*](#)
969 [Science Letters 404, 332–343.](#)

970 [Wilkinson B. H. and Ivany L. C. \(2002\) Paleoclimatic inference from stable isotope profiles of](#)
971 [accretionary biogenic hardparts – a quantitative approach to the evaluation of incomplete data.](#)
972 [Palaeogeography, Palaeoclimatology, Palaeoecology](#) **185**, 95–114.

973 [de Winter N., Vellekoop J., Vorsselmans R., Golreihan A., Soete J., Petersen S., Meyer K., Casadio](#)
974 [S., Speijer R. and Claeys P. \(2018\) An assessment of latest Cretaceous Pycnodonte vesicularis](#)
975 [\(Lamarck, 1806\) shells as records for palaeoseasonality: a multi-proxy investigation.](#) *Climate of the*
976 *Past* **14**, 725–749.

977 [de Winter N. J., Agterhuis T. and Ziegler M. \(2021\) Optimizing sampling strategies in high-resolution](#)
978 [paleoclimate records.](#) *Climate of the Past* **17**, 1315–1340.

979 [de Winter N. J., Goderis S., Dehairs F., Jagt J. W., Fraaije R. H., Van Malderen S. J., Vanhaecke F.](#)
980 [and Claeys P. \(2017\) Tropical seasonality in the late Campanian \(late Cretaceous\): Comparison](#)
981 [between multiproxy records from three bivalve taxa from Oman.](#) *Palaeogeography, Palaeoclimatology,*
982 *Palaeoecology* **485**, 740–760.

983 [de Winter N. J., Goderis S., Malderen S. J. M. V., Sinnesael M., Vansteenberge S., Snoeck C., Belza](#)
984 [J., Vanhaecke F. and Claeys P. \(2020a\) Subdaily-Scale Chemical Variability in a *Torreites Sanchezi*](#)
985 [Rudist Shell: Implications for Rudist Paleobiology and the Cretaceous Day-Night Cycle.](#)
986 [Paleoceanography and Paleoclimatology](#) **35**, e2019PA003723.

987 [de Winter N. J., Ullmann C. V., Sørensen A. M., Thibault N., Goderis S., Van Malderen S. J. M.,](#)
988 [Snoeck C., Goolaerts S., Vanhaecke F. and Claeys P. \(2020b\) Shell chemistry of the boreal](#)
989 [Campanian bivalve *Rastellum diluvianum* \(Linnaeus, 1767\) reveals temperature](#)
990 [seasonality, growth rates and life cycle of an extinct Cretaceous oyster.](#) *Biogeosciences* **17**, 2897–
991 *2922*.

992 [de Winter N. J., Vellekoop J., Clark A. J., Stassen P., Speijer R. P. and Claeys P. \(2020c\) The giant](#)
993 [marine gastropod *Campanile giganteum* \(Lamarck, 1804\) as a high-resolution archive of seasonality in](#)
994 [the Eocene greenhouse world.](#) *Geochemistry, Geophysics, Geosystems* **21**, e2019GC008794.

995 [Xu C., Zheng H., Nakatsuka T., Sano M., Li Z. and Ge J. \(2016\) Inter- and intra-annual tree-ring](#)
996 [cellulose oxygen isotope variability in response to precipitation in Southeast China.](#) *Trees* **30**, 785–
997 *794*.

998 [Yan H., Liu C., An Z., Yang W., Yang Yuanjian, Huang P., Qiu S., Zhou P., Zhao N., Fei H., Ma X., Shi](#)
999 [G., Dodson J., Hao J., Yu K., Wei G., Yang Yanan, Jin Z. and Zhou W. \(2020\) Extreme weather](#)
1000 [events recorded by daily to hourly resolution biogeochemical proxies of marine giant clam shells.](#)
1001 [PNAS](#) **117**, 7038–7043.

1002 [Zhu F., Emile-Geay J., McKay N. P., Hakim G. J., Khider D., Ault T. R., Steig E. J., Dee S. and](#)
1003 [Kirchner J. W. \(2019\) Climate models can correctly simulate the continuum of global-average](#)
1004 [temperature variability.](#) *PNAS* **116**, 8728–8733.

1005 [Bajnai, D., Guo, W., Spötl, C., Coplen, T. B., Methner, K., Löffler, N., Krsnik, E., Gischler, E., Hansen,](#)
1006 [M., Henkel, D., Price, G. D., Raddatz, J., Scholz, D. and Fiebig, J.: Dual clumped isotope thermometry](#)
1007 [resolves kinetic biases in carbonate formation temperatures, Nature Communications, 11\(1\), 4005,](#)
1008 [doi:10.1038/s41467-020-17501-0, 2020.](#)

1009 [Baldini, J. U. L., McDermott, F., Hoffmann, D. L., Richards, D. A. and Clipson, N.: Very high frequency](#)
1010 [and seasonal cave atmosphere PCO₂ variability: Implications for stalagmite growth and oxygen](#)
1011 [isotope-based paleoclimate records, Earth and Planetary Science Letters, 272\(1\), 118–129,](#)
1012 [doi:10.1016/j.epsl.2008.04.031, 2008.](#)

1013 [Brand, W. A., Coplen, T. B., Vogl, J., Rosner, M. and Prohaska, T.: Assessment of international](#)
1014 [reference materials for isotope ratio analysis \(IUPAC Technical Report\), Pure and Applied Chemistry,](#)
1015 [86\(3\), 425–467, doi:10.1515/pac-2013-1023, 2014.](#)

1016 de Brauwere, A., De Ridder, F., Pintelon, R., Schoukens, J. and Dehairs, F.: A comparative study of
1017 methods to reconstruct a periodic time series from an environmental proxy record, *Earth Science*
1018 *Reviews*, 95(3), 97–118, doi:[10.1016/j.earscirev.2009.04.002](https://doi.org/10.1016/j.earscirev.2009.04.002), 2009.

1019 Butler, P. G., Wanamaker, A. D., Scourse, J. D., Richardson, C. A. and Reynolds, D. J.: Variability of
1020 marine climate on the North Icelandic Shelf in a 1357 year proxy archive based on growth increments
1021 in the bivalve *Arctica islandica*, *Palaeogeography, Palaeoclimatology, Palaeoecology*, 373, 141–151,
1022 doi:[10.1016/j.palaeo.2012.01.016](https://doi.org/10.1016/j.palaeo.2012.01.016), 2013.

1023 Chauvaud, L., Lorrain, A., Dunbar, R. B., Paulet, Y. M., Thouzeau, G., Jean, F., Guarini, J. M. and
1024 Mucciarone, D.: Shell of the Great Scallop *Pecten maximus* as a high frequency archive of
1025 paleoenvironmental changes, *Geochemistry, Geophysics, Geosystems*, 6(8),
1026 doi:[10.1029/2004GC000890](https://doi.org/10.1029/2004GC000890), 2005.

1027 Coplen, T. B.: Calibration of the calcite–water oxygen isotope geothermometer at Devils Hole,
1028 Nevada, a natural laboratory, *Geochimica et Cosmochimica Acta*, 71(16), 3948–3957,
1029 doi:[10.1016/j.gca.2007.05.028](https://doi.org/10.1016/j.gca.2007.05.028), 2007.

1030 Daëron, M., Guo, W., Eiler, J., Genty, D., Blamart, D., Boch, R., Drysdale, R., Maire, R., Wainer, K. and
1031 Zanchetta, G.: $^{13}\text{C}^{18}\text{O}$ clumping in speleothems: Observations from natural caves and precipitation
1032 experiments, *Geochimica et Cosmochimica Acta*, 75(12), 3303–3317, doi:[10.1016/j.gca.2010.10.032](https://doi.org/10.1016/j.gca.2010.10.032),
1033 2011.

1034 Daëron, M., Drysdale, R. N., Peral, M., Huyghe, D., Blamart, D., Coplen, T. B., Lartaud, F. and
1035 Zanchetta, G.: Most Earth surface calcites precipitate out of isotopic equilibrium, *Nature*
1036 *Communications*, 10(1), 429, doi:[10.1038/s41467-019-08336-5](https://doi.org/10.1038/s41467-019-08336-5), 2019.

1037 De Ridder, F., de Brauwere, A., Pintelon, R., Schoukens, J., Dehairs, F., Baeyens, W. and Wilkinson, B.
1038 H.: Comment on: Paleoclimatic inference from stable isotope profiles of accretionary biogenic
1039 hardparts—a quantitative approach to the evaluation of incomplete data, by Wilkinson, BH, Ivany,
1040 LC, 2002. *Palaeogeogr. Palaeoclimatol. Palaeoecol.* 185, 95–114, *Palaeogeography, Palaeoclimatology,*
1041 *Palaeoecology*, 248(3–4), 473–476, 2007.

1042 DeCarlo, T. M. and Cohen, A. L.: Dissepiments, density bands and signatures of thermal stress in
1043 *Porites* skeletons, *Coral Reefs*, 36(3), 749–761, doi:[10.1007/s00338-017-1566-9](https://doi.org/10.1007/s00338-017-1566-9), 2017.

1044 Dettman, D. L., Reische, A. K. and Lohmann, K. C.: Controls on the stable isotope composition of
1045 seasonal growth bands in aragonitic fresh-water bivalves (Unionidae), *Geochimica et Cosmochimica*
1046 *Acta*, 63(7–8), 1049–1057, 1999.

1047 Duan, Q., Sorooshian, S. and Gupta, V.: Effective and efficient global optimization for conceptual
1048 rainfall runoff models, *Water resources research*, 28(4), 1015–1031, 1992.

1049 Dunbar, R. B. and Wellington, G. M.: Stable isotopes in a branching coral monitor seasonal
1050 temperature variation, *Nature*, 293(5832), 453–455, 1981.

1051 Durham, S. R., Gillikin, D. P., Goodwin, D. H. and Dietl, G. P.: Rapid determination of oyster lifespans
1052 and growth rates using LA-ICP-MS line scans of shell Mg/Ca ratios, *Palaeogeography,*
1053 *Palaeoclimatology, Palaeoecology*, 2017.

1054 Epstein, S., Buchsbaum, R., Lowenstam, H. A. and Urey, H. C.: Revised carbonate–water isotopic
1055 temperature scale, *Geological Society of America Bulletin*, 64(11), 1315–1326, 1953.

1056 Fairchild, I. J., Smith, C. L., Baker, A., Fuller, L., Spötl, C., Matthey, D., McDermott, F. and others:
1057 Modification and preservation of environmental signals in speleothems, *Earth Science Reviews*,
1058 75(1), 105–153, 2006.

1059 Frisia, S., Borsato, A., Fairchild, I. J. and McDermott, F.: Calcite fabrics, growth mechanisms, and
1060 environments of formation in speleothems from the Italian Alps and southwestern Ireland, *Journal of*
1061 *Sedimentary Research*, 70(5), 1183–1196, 2000.

1062 Gagan, M. K., Chivas, A. R. and Isdale, P. J.: High-resolution isotopic records from corals using ocean
1063 temperature and mass-spawning chronometers, *Earth and Planetary Science Letters*, 121(3–4), 549–
1064 558, doi:[10.1016/0012-821X\(94\)90090-6](https://doi.org/10.1016/0012-821X(94)90090-6), 1994.

1065 Goodwin, D. H., Schöne, B. R. and Dettman, D. L.: Resolution and Fidelity of Oxygen Isotopes as
1066 Paleotemperature Proxies in Bivalve Mollusk Shells: Models and Observations, *PALAIOS*, 18(2), 110–
1067 125, doi:[10.1669/0883-1351\(2003\)18<110:RAFOQI>2.0.CO;2](https://doi.org/10.1669/0883-1351(2003)18<110:RAFOQI>2.0.CO;2), 2003.

1068 Goodwin, D. H., Paul, P. and Wissink, C. L.: MoGroFunGen: A numerical model for reconstructing
1069 intra-annual growth rates of bivalve molluscs, *Palaeogeography, Palaeoclimatology, Palaeoecology*,
1070 276(1), 47–55, doi:[10.1016/j.palaeo.2009.02.026](https://doi.org/10.1016/j.palaeo.2009.02.026), 2009.

1071 Grossman, E. L. and Ku, T. L.: Oxygen and carbon isotope fractionation in biogenic aragonite:
1072 temperature effects, *Chemical Geology: Isotope Geoscience section*, 59, 59–74, 1986.

1073 Huybers, P. and Curry, W.: Links between annual, Milankovitch and continuum temperature
1074 variability, *Nature*, 441(7091), 329, 2006.

1075 Huyghe, D., de Rafelis, M., Ropert, M., Mouchi, V., Emmanuel, L., Renard, M. and Lartaud, F.: New
1076 insights into oyster high-resolution hinge growth patterns, *Mar Biol*, 166(4), 48, doi:[10.1007/s00227-019-3496-2](https://doi.org/10.1007/s00227-019-3496-2), 2019.

1078 IPCC: GLOBAL WARMING OF 1.5 °C an IPCC special report on the impacts of global warming of 1.5 °C
1079 above pre-industrial levels and related global greenhouse gas emission pathways, in the context of
1080 strengthening the global response to the threat of climate change, sustainable development, and
1081 efforts to eradicate poverty. [online] Available from:
1082 http://report.ipcc.ch/sr15/pdf/sr15_spm_final.pdf, 2018.

1083 Ivany, L. C. and Runnegar, B.: Early Permian seasonality from bivalve $\delta^{18}\text{O}$ and implications for the
1084 oxygen isotopic composition of seawater, *Geology*, 38(11), 1027–1030, 2010.

1085 Jones, D. S.: Sclerochronology: Reading the Record of the Molluscan Shell: Annual growth increments
1086 in the shells of bivalve molluscs record marine climatic changes and reveal surprising longevity,
1087 *American Scientist*, 71(4), 384–391, 1983.

1088 Jones, D. S. and Quitmyer, I. R.: Marking Time with Bivalve Shells: Oxygen Isotopes and Season of
1089 Annual Increment Formation, *PALAIOS*, 11(4), 340–346, doi:[10.2307/3515244](https://doi.org/10.2307/3515244), 1996.

1090 Judd, E. J., Wilkinson, B. H. and Ivany, L. C.: The life and time of clams: Derivation of intra-annual
1091 growth rates from high-resolution oxygen isotope profiles, *Palaeogeography, Palaeoclimatology,*
1092 *Palaeoecology*, 490, 70–83, 2018.

1093 Kim, S. T. and O'Neil, J. R.: Equilibrium and nonequilibrium oxygen isotope effects in synthetic
1094 carbonates, *Geochimica et Cosmochimica Acta*, 61(16), 3461–3475, doi:[10.1016/S0016-7037\(97\)00169-5](https://doi.org/10.1016/S0016-7037(97)00169-5), 1997.

1096 Lachniet, M. S.: Climatic and environmental controls on speleothem oxygen isotope values,
1097 *Quaternary Science Reviews*, 28(5–6), 412–432, 2009.

1098 Le Tissier, M. D. A., Clayton, B., Brown, B. E. and Davis, P. S.: Skeletal correlates of coral density
1099 banding and an evaluation of radiography as used in sclerochronology, *Marine Ecology Progress
1100 Series*, 110(1), 29–44, 1994.

1101 LeGrande, A. N. and Schmidt, G. A.: Global gridded data set of the oxygen isotopic composition in
1102 seawater, *Geophysical research letters*, 33(12), 2006.

1103 Lough, J. M.: Climate records from corals, *WIREs Climate Change*, 1(3), 318–331, doi:[10.1002/wcc.39](https://doi.org/10.1002/wcc.39),
1104 2010.

1105 Mahé, K., Bellamy, E., Lartaud, F. and Rafélis, M. de: Calcein and manganese experiments for marking
1106 the shell of the common cockle (*Cerastoderma edule*): tidal rhythm validation of increments
1107 formation, *Aquat. Living Resour.*, 23(3), 239–245, doi:[10.1051/alr/2010025](https://doi.org/10.1051/alr/2010025), 2010.

1108 Matthey, D., Lowry, D., Duffet, J., Fisher, R., Hodge, E. and Frisia, S.: A 53-year seasonally resolved
1109 oxygen and carbon isotope record from a modern Gibraltar speleothem: Reconstructed drip water
1110 and relationship to local precipitation, *Earth and Planetary Science Letters*, 269(1), 80–95,
1111 doi:[10.1016/j.epsl.2008.01.051](https://doi.org/10.1016/j.epsl.2008.01.051), 2008.

1112 McCrea, J. M.: On the Isotopic Chemistry of Carbonates and a Paleotemperature Scale, *J. Chem.
1113 Phys.*, 18(6), 849–857, doi:[10.1063/1.1747785](https://doi.org/10.1063/1.1747785), 1950.

1114 Mitchell Jr., J. M.: An overview of climatic variability and its causal mechanisms, *Quaternary
1115 Research*, 6(4), 481–493, doi:[10.1016/0033-5894\(76\)90021-1](https://doi.org/10.1016/0033-5894(76)90021-1), 1976.

1116 Mohr, R. C., Tobin, T. S., Petersen, S. V., Dutton, A. and Oliphant, E.: Subannual stable isotope records
1117 reveal climate warming and seasonal anoxia associated with two extinction intervals across the
1118 Cretaceous–Paleogene boundary on Seymour Island, Antarctica, *Geology*, 48(11), 1131–1136,
1119 doi:[10.1130/G47758.1](https://doi.org/10.1130/G47758.1), 2020.

1120 Müller, P., Taylor, M. H., Klicpera, A., Wu, H. C., Michel, J. and Westphal, H.: Food for thought:
1121 Mathematical approaches for the conversion of high-resolution sclerochronological oxygen isotope
1122 records into sub-annually resolved time series, *Palaeogeography, Palaeoclimatology, Palaeoecology*,
1123 440, 763–776, doi:[10.1016/j.palaeo.2015.09.032](https://doi.org/10.1016/j.palaeo.2015.09.032), 2015.

1124 O'Donnell, M. S. and Ignizio, D. A.: Bioclimatic predictors for supporting ecological applications in the
1125 conterminous United States, *US Geological Survey Data Series*, 691(10), 2012.

1126 Ommen, T. D. van and Morgan, V.: Calibrating the ice core paleothermometer using seasonality,
1127 *Journal of Geophysical Research: Atmospheres*, 102(D8), 9351–9357, doi:[10.1029/96JD04014](https://doi.org/10.1029/96JD04014), 1997.

1128 Poussart, P. M., Myneni, S. C. B. and Lanzirrotti, A.: Tropical dendrochemistry: A novel approach to
1129 estimate age and growth from ringless trees, *Geophysical Research Letters*, 33(17),
1130 doi:[10.1029/2006GL026929](https://doi.org/10.1029/2006GL026929), 2006.

1131 R Core Team: R: A Language and Environment for Statistical Computing, R Foundation for Statistical
1132 Computing, Vienna, Austria. [online] Available from: <https://www.R-project.org/>, 2020.

1133 Rohling, E. J.: Oxygen isotope composition of seawater, *The Encyclopedia of Quaternary Science*.
1134 Amsterdam: Elsevier, 2, 915–922, 2013.

1135 Rollion-Bard, C., Chaussidon, M. and France-Lanord, C.: pH control on oxygen isotopic composition of
1136 symbiotic corals, *Earth and Planetary Science Letters*, 215(1), 275–288, doi:[10.1016/S0012-
1137 821X\(03\)00391-1](https://doi.org/10.1016/S0012-821X(03)00391-1), 2003.

1138 Saenger, C., Gabitov, R. I., Farmer, J., Watkins, J. M. and Stone, R.: Linear correlations in bamboo
1139 coral $\delta^{13}\text{C}$ and $\delta^{18}\text{O}$ sampled by SIMS and micromill: Evaluating paleoceanographic potential and
1140 biomineralization mechanisms using $\delta^{11}\text{B}$ and $\Delta 47$ composition, *Chemical Geology*, 454, 1–14,
1141 doi:[10.1016/j.chemgeo.2017.02.014](https://doi.org/10.1016/j.chemgeo.2017.02.014), 2017.

1142 Sano, Y., Kobayashi, S., Shirai, K., Takahata, N., Matsumoto, K., Watanabe, T., Sowa, K. and Iwai, K.:
1143 Past daily light cycle recorded in the strontium/calcium ratios of giant clam shells, *Nature
1144 Communications*, 3, 761, 2012.

1145 Schöne, B. R. and Gillikin, D. P.: Unraveling environmental histories from skeletal diaries — Advances
1146 in sclerochronology, *Palaeogeography, Palaeoclimatology, Palaeoecology*, 373, 1–5,
1147 doi:[10.1016/j.palaeo.2012.11.026](https://doi.org/10.1016/j.palaeo.2012.11.026), 2013.

1148 Schöne, B. R., Fiebig, J., Pfeiffer, M., Gleß, R., Hickson, J., Johnson, A. L., Dreyer, W. and Oschmann,
1149 W.: Climate records from a bivalved Methuselah (*Arctica islandica*, Mollusca; Iceland),
1150 *Palaeogeography, Palaeoclimatology, Palaeoecology*, 228(1–2), 130–148, 2005.

1151 Schöne, B. R., Zhang, Z., Radermacher, P., Thébault, J., Jacob, D. E., Nunn, E. V. and Maurer, A.-F.:
1152 Sr/Ca and Mg/Ca ratios of ontogenetically old, long-lived bivalve shells (*Arctica islandica*) and their
1153 function as paleotemperature proxies, *Palaeogeography, Palaeoclimatology, Palaeoecology*, 302(1–
1154 2), 52–64, 2011.

1155 Sinnesael, M., De Vleeschouwer, D., Zeeden, C., Batenburg, S. J., Da Silva, A. C., de Winter, N. J.,
1156 Dinarès-Turell, J., Drury, A. J., Gambacorta, G. and Hilgen, F. J.: The Cyclostratigraphy
1157 Intercomparison Project (CIP): consistency, merits and pitfalls, *Earth Science Reviews*, 102965, 2019.

1158 Sosdian, S., Gentry, D. K., Lear, C. H., Grossman, E. L., Hicks, D. and Rosenthal, Y.: Strontium to
1159 calcium ratios in the marine gastropod *Conus ermineus*: Growth rate effects and temperature
1160 calibration, *Geochemistry, Geophysics, Geosystems*, 7(11), 2006.

1161 Steuber, T., Rauch, M., Masse, J. P., Graaf, J. and Malkoč, M.: Low latitude seasonality of Cretaceous
1162 temperatures in warm and cold episodes, *Nature*, 437(7063), 1341–1344, 2005.

1163 Superville, P. J., De Winter, N., Phung, A. T., Proix, N., Baeyens, W. and Gao, Y.: Radial metal
1164 concentration profiles in trees growing on highly contaminated soils, *Chemosphere*, 172, 80–88,
1165 doi:[10.1016/j.chemosphere.2016.12.142](https://doi.org/10.1016/j.chemosphere.2016.12.142), 2017.

1166 Tarutani, T., Clayton, R. N. and Mayeda, T. K.: The effect of polymorphism and magnesium
1167 substitution on oxygen isotope fractionation between calcium carbonate and water, *Geochimica et
1168 Cosmochimica Acta*, 33(8), 987–996, doi:[10.1016/0016-7037\(69\)90108-2](https://doi.org/10.1016/0016-7037(69)90108-2), 1969.

1169 Treble, P. C., Schmitt, A. K., Edwards, R. L., McKeegan, K. D., Harrison, T. M., Grove, M., Cheng, H. and
1170 Wang, Y. J.: High resolution Secondary Ionisation Mass Spectrometry (SIMS) $\delta^{18}\text{O}$ analyses of Hulu
1171 Cave speleothem at the time of Heinrich Event 1, *Chemical Geology*, 238(3), 197–212,
1172 doi:[10.1016/j.chemgeo.2006.11.009](https://doi.org/10.1016/j.chemgeo.2006.11.009), 2007.

1173 Uchikawa, J. and Zeebe, R. E.: The effect of carbonic anhydrase on the kinetics and equilibrium of the
1174 oxygen isotope exchange in the $\text{CO}_2\text{--H}_2\text{O}$ system: Implications for $\delta^{18}\text{O}$ vital effects in biogenic
1175 carbonates, *Geochimica et Cosmochimica Acta*, 95, 15–34, 2012.

1176 Ullmann, C. V. and Korte, C.: Diagenetic alteration in low-Mg calcite from macrofossils: a review,
1177 *Geological Quarterly*, 59(1), 3–20, 2015.

1178 Ullmann, C. V., Wiechert, U. and Korte, C.: Oxygen isotope fluctuations in a modern North Sea oyster
1179 (*Crassostrea gigas*) compared with annual variations in seawater temperature: Implications for
1180 palaeoclimate studies, *Chemical Geology*, 277(1), 160–166, 2010.

1181 Ullmann, C. V., Böhm, F., Rickaby, R. E., Wiechert, U. and Korte, C.: The Giant Pacific Oyster
1182 (*Crassostrea gigas*) as a modern analog for fossil ostreoids: isotopic (Ca, O, C) and elemental (Mg/Ca,
1183 Sr/Ca, Mn/Ca) proxies, *Geochemistry, Geophysics, Geosystems*, 14(10), 4109–4120, 2013.

1184 Urban, F. E., Cole, J. E. and Overpeck, J. T.: Influence of mean climate change on climate variability
1185 from a 155-year tropical Pacific coral record, *Nature*, 407(6807), 989–993, doi:[10.1038/35039597](https://doi.org/10.1038/35039597),
1186 2000.

1187 Urey, H. C.: Oxygen Isotopes in Nature and in the Laboratory, *Science*, 108(2810), 489–496, 1948.

1188 Van Rampelbergh, M., Verheyden, S., Allan, M., Quinif, Y., Keppens, E. and Claeys, P.: Seasonal
1189 variations recorded in cave monitoring results and a 10-year monthly resolved speleothem $\delta^{18}\text{O}$ and
1190 $\delta^{13}\text{C}$ record from the Han sur Lesse cave, Belgium, *Climate of the Past Discussions*, 10, 1821–1856,
1191 2014.

1192 Vansteenberge, S., Verheyden, S., Cheng, H., Edwards, R. L., Keppens, E. and Claeys, P.: Paleoclimate
1193 in continental northwestern Europe during the Eemian and early Weichselian (125–97 ka): insights
1194 from a Belgian speleothem, *Clim. Past*, 12(7), 1445–1458, doi:[10.5194/cp-12-1445-2016](https://doi.org/10.5194/cp-12-1445-2016), 2016.

1195 Vansteenberge, S., Winter, N. de, Sinnesael, M., Verheyden, S., Goderis, S., Malderen, S. J. M. V.,
1196 Vanhaecke, F. and Claeys, P.: Reconstructing seasonality through stable isotope and trace element
1197 analysis of the Proserpine stalagmite, Han-sur-Lesse Cave, Belgium: indications for climate-driven
1198 changes during the last 400 years, *Climate of the Past Discussions*, 1–32,
1199 doi:<https://doi.org/10.5194/cp-2019-78>, 2019.

1200 Verheyden, S., Baele, J. M., Keppens, E., Genty, D., Cattani, O., Cheng, H., LAWRENCE, E., ZHANG, H.,
1201 Van Strijdonck, M. and Quinif, Y.: The Proserpine stalagmite (Han-Sur-Lesse Cave, Belgium):
1202 preliminary environmental interpretation of the last 1000 years as recorded in a layered speleothem,
1203 *Geologica Belgica*, 2006.

1204 de Villiers, S., Nelson, B. K. and Chivas, A. R.: Biological controls on coral Sr/Ca and $\delta^{18}\text{O}$
1205 reconstructions of sea surface temperatures, *Science*, 269(5228), 1247, 1995.

1206 Wang, Y. J., Cheng, H., Edwards, R. L., An, Z. S., Wu, J. Y., Shen, C. C. and Dorale, J. A.: A High-
1207 Resolution Absolute Dated Late Pleistocene Monsoon Record from Hulu Cave, China, *Science*,
1208 294(5550), 2345–2348, doi:[10.1126/science.1064618](https://doi.org/10.1126/science.1064618), 2001.

1209 Watkins, J. M., Hunt, J. D., Ryerson, F. J. and DePaolo, D. J.: The influence of temperature, pH, and
1210 growth rate on the $\delta^{18}\text{O}$ composition of inorganically precipitated calcite, *Earth and Planetary
1211 Science Letters*, 404, 332–343, doi:[10.1016/j.epsl.2014.07.036](https://doi.org/10.1016/j.epsl.2014.07.036), 2014.

1212 Wilkinson, B. H. and Ivany, L. C.: Paleoclimatic inference from stable isotope profiles of accretionary
1213 biogenic hardparts – a quantitative approach to the evaluation of incomplete data, *Palaeogeography,
1214 Palaeoclimatology, Palaeoecology*, 185(1), 95–114, doi:[10.1016/S0031-0182\(02\)00279-1](https://doi.org/10.1016/S0031-0182(02)00279-1), 2002.

1215 de Winter, N. J., Goderis, S., Dehairs, F., Jagt, J. W., Fraaije, R. H., Van Malderen, S. J., Vanhaecke, F.
1216 and Claeys, P.: Tropical seasonality in the late Campanian (late Cretaceous): Comparison between

1217 multiproxy records from three bivalve taxa from Oman, *Palaeogeography, Palaeoclimatology,*
1218 *Palaeoecology*, 485, 740–760, 2017.

1219 de Winter, N., Vellekoop, J., Vorsselmans, R., Golreihan, A., Soete, J., Petersen, S., Meyer, K., Casadio,
1220 S., Speijer, R. and Claeys, P.: An assessment of latest Cretaceous *Pycnodonte vesicularis* (Lamarck,
1221 1806) shells as records for palaeoseasonality: a multi-proxy investigation, *Climate of the Past*, 14(6),
1222 725–749, 2018.

1223 de Winter, N. J., Goderis, S., Malderen, S. J. M. V., Sinnesael, M., Vansteenberge, S., Snoeck, C., Belza,
1224 J., Vanhaecke, F. and Claeys, P.: Subdaily Scale Chemical Variability in a *Torreites Sanchezi* Rudist
1225 Shell: Implications for Rudist Paleobiology and the Cretaceous Day-Night Cycle, *Paleoceanography*
1226 and *Paleoclimatology*, 35(2), e2019PA003723, doi:[10.1029/2019PA003723](https://doi.org/10.1029/2019PA003723), 2020a.

1227 de Winter, N. J., Ullmann, C. V., Sørensen, A. M., Thibault, N., Goderis, S., Van Malderen, S. J. M.,
1228 Snoeck, C., Goolaerts, S., Vanhaecke, F. and Claeys, P.: Shell chemistry of the boreal Campanian
1229 bivalve *Rastellum diluvianum*; (Linnaeus, 1767) reveals temperature seasonality, growth rates and
1230 life cycle of an extinct Cretaceous oyster, *Biogeosciences*, 17(11), 2897–2922, doi:[10.5194/bg-17-](https://doi.org/10.5194/bg-17-2897-2020)
1231 [2897-2020](https://doi.org/10.5194/bg-17-2897-2020), 2020b.

1232 de Winter, N. J., Vellekoop, J., Clark, A. J., Stassen, P., Speijer, R. P. and Claeys, P.: The giant marine
1233 gastropod *Campanile giganteum* (Lamarck, 1804) as a high-resolution archive of seasonality in the
1234 Eocene greenhouse world, *Geochemistry, Geophysics, Geosystems*, n/a(n/a), e2019GC008794,
1235 doi:[10.1029/2019GC008794](https://doi.org/10.1029/2019GC008794), 2020c.

1236 de Winter, N., Agterhuis, T. and Ziegler, M.: Optimizing sampling strategies in high-resolution
1237 paleoclimate records, *Climate of the Past Discussions*, 1–52, doi:[https://doi.org/10.5194/cp-2020-](https://doi.org/10.5194/cp-2020-118)
1238 [118](https://doi.org/10.5194/cp-2020-118), 2020d.

1239 Xu, C., Zheng, H., Nakatsuka, T., Sano, M., Li, Z. and Ge, J.: Inter- and intra-annual tree-ring cellulose
1240 oxygen isotope variability in response to precipitation in Southeast China, *Trees*, 30(3), 785–794,
1241 2016.

1242 Yan, H., Liu, C., An, Z., Yang, W., Yang, Y., Huang, P., Qiu, S., Zhou, P., Zhao, N., Fei, H., Ma, X., Shi, G.,
1243 Dodson, J., Hao, J., Yu, K., Wei, G., Yang, Y., Jin, Z. and Zhou, W.: Extreme weather events recorded by
1244 daily to hourly resolution biogeochemical proxies of marine giant clam shells, *PNAS*, 117(13), 7038–
1245 7043, doi:[10.1073/pnas.1916784117](https://doi.org/10.1073/pnas.1916784117), 2020.

1246 Zeebe, R. E.: An expression for the overall oxygen isotope fractionation between the sum of dissolved
1247 inorganic carbon and water, *Geochemistry, Geophysics, Geosystems*, 8(9),
1248 doi:[10.1029/2007GC001663](https://doi.org/10.1029/2007GC001663), 2007.

1249 Zhu, F., Emile-Geay, J., McKay, N. P., Hakim, G. J., Khider, D., Ault, T. R., Steig, E. J., Dee, S. and
1250 Kirchner, J. W.: Climate models can correctly simulate the continuum of global-average temperature
1251 variability, *PNAS*, 116(18), 8728–8733, doi:[10.1073/pnas.1809959116](https://doi.org/10.1073/pnas.1809959116), 2019.